

Balancing Geometry and Density: Path Distances on High-Dimensional Data

Anna Little*

Daniel McKenzie†

James M. Murphy‡

December 3, 2021

Abstract

New geometric and computational analyses of power-weighted shortest-path distances (PWSPDs) are presented. By illuminating the way these metrics balance density and geometry in the underlying data, we clarify their key parameters and discuss how they may be chosen in practice. Comparisons are made with related data-driven metrics, which illustrate the broader role of density in kernel-based unsupervised and semi-supervised machine learning. Computationally, we relate PWSPDs on complete weighted graphs to their analogues on weighted nearest neighbor graphs, providing high probability guarantees on their equivalence that are near-optimal. Connections with percolation theory are developed to establish estimates on the bias and variance of PWSPDs in the finite sample setting. The theoretical results are bolstered by illustrative experiments, demonstrating the versatility of PWSPDs for a wide range of data settings. Throughout the paper, our results require only that the underlying data is sampled from a low-dimensional manifold, and depend crucially on the intrinsic dimension of this manifold, rather than its ambient dimension.

1 Introduction

The analysis of high-dimensional data is a crucial challenge in modern statistical and machine learning. In order to defeat the *curse of dimensionality* [31, 27, 9], distance metrics that efficiently and accurately capture intrinsically low-dimensional latent structure in the high-dimensional data are required. Indeed, this need to capture low-dimensional linear and nonlinear structure in data has led to the development of a range of data-dependent distances and related dimension reduction methods, which have been widely employed in applications [36, 48, 7, 21, 17, 49]. Understanding how these metrics trade off fundamental properties in the data (e.g. local versus global structure, geometry versus density) when making pointwise comparisons is an important challenge in their use, and may be understood as a form of model selection in unsupervised and semisupervised machine learning problems.

1.1 Power-Weighted Shortest Path Distances

In this paper we analyze *power-weighted shortest path distances* (PWSPDs) and develop their applications to problems in machine learning. These metrics compute the shortest path between two points in the data, accounting for the underlying density of the points along the path. Paths through

*Department of Mathematics, University of Utah, Salt Lake City, UT 84112, USA (little@math.utah.edu)

†Department of Mathematics, UCLA, Los Angeles, CA 90095, USA (mckenzie@math.ucla.edu)

‡Department of Mathematics, Tufts University, Medford, MA 02155, USA (jm.murphy@tufts.edu)

low-density regions are penalized, so that the optimal path must balance being “short” (in the sense of the classical geodesic distance) with passing through high-density regions. We consider a finite data set $\mathcal{X} = \{x_i\}_{i=1}^n \subset \mathbb{R}^D$, which we usually assume to be intrinsically low-dimensional, in the sense that there exists a d -dimensional Riemannian *data manifold* $\mathcal{M} \subset \mathbb{R}^D$ and a probability density function $f(x)$ supported on \mathcal{M} such that $\{x_i\}_{i=1}^n \stackrel{i.i.d.}{\sim} f(x)$.

Definition 1.1. For $p \in [1, \infty)$ and for $x, y \in \mathcal{X}$, the (discrete) p -weighted shortest path distance (PWSPD) from x to y is:

$$\ell_p(x, y) = \min_{\pi = \{x_i\}_{i=1}^L} \left(\sum_{i=1}^{L-1} \|x_i - x_{i+1}\|^p \right)^{\frac{1}{p}}, \quad (1)$$

where π is a path consisting of data points in \mathcal{X} with $x_1 = x$ and $x_L = y$.

Early uses of density-based distances for interpolation [45] led to the formulation of PWSPD in the context of unsupervised and semisupervised learning and applications [24, 50, 13, 44, 14, 11, 39, 38, 34, 53, 12]. It will occasionally be useful to think of $\ell_p(\cdot, \cdot)$ as the path distance in the complete graph on \mathcal{X} with edge weights $\|x_i - x_j\|^p$, which we shall denote $\mathcal{G}_{\mathcal{X}}^p$. When $p = 1$, $\ell_1(x, y) = \|x - y\|$, i.e. the Euclidean distance. As p increases, the largest elements in the set of path edge lengths $\{\|x_i - x_{i+1}\|\}_{i=1}^{L-1}$ begin to dominate the optimization, so that paths through higher density regions (with shorter edge lengths) are promoted. When $p \rightarrow \infty$, ℓ_p converges (up to rescaling) to the longest-leg path distance $\ell_\infty(x, y) = \min_{\pi = \{x_i\}_{i=1}^L} \max_{i=1, \dots, L-1} \|x_i - x_{i+1}\|$ [34] and is thus driven by the density function f . Outside these extremes, ℓ_p balances taking a “short” path and taking one through regions of high-density. Note that ℓ_p can be defined for $p < 1$, but it does not satisfy the triangle inequality and is thus not a metric (ℓ_p^p however *is* a metric for all $p > 0$). This case was studied in [1], where it is demonstrated to have counterintuitive properties that should preclude its use in machine learning.

While (1) is defined for finite data, it admits a corresponding continuum formulation.

Definition 1.2. For $p \in [1, \infty)$, a density function f on a d -dimensional Riemannian manifold (\mathcal{M}, g) , and any $x, y \in \mathcal{M}$, the (continuous) p -weighted shortest path distance from x to y is:

$$\mathcal{L}_p(x, y) = \left(\inf_{\gamma} \int_0^1 \frac{1}{f(\gamma(t))^{\frac{p-1}{d}}} \sqrt{g(\gamma'(t), \gamma'(t))} dt \right)^{\frac{1}{p}}, \quad (2)$$

where $\gamma : [0, 1] \rightarrow \mathcal{M}$ is a C^1 path with $\gamma(0) = x, \gamma(1) = y$.

Note \mathcal{L}_1 is simply geodesic distance on \mathcal{M} . However for $p > 1$ and a nonuniform density, the optimal path γ is generally not the shortest path: \mathcal{L}_p favors paths which travel along high-density ridges, and detours off the classical \mathcal{L}_1 geodesics are thus acceptable. The parameter p controls how large of a detour is acceptable; for large p , optimal paths may become highly nonlocal.

It is known [32, 26] that for $p > 1$ and all $x, y \in \mathcal{M}$,

$$\lim_{n \rightarrow \infty} n^{\frac{p-1}{pd}} \ell_p(x, y) = C_{p,d} \mathcal{L}_p(x, y) \quad (3)$$

for an absolute constant $C_{p,d}$ depending only on p and d , i.e. that the discrete PWSPD (appropriately rescaled) is a consistent estimator for the continuum PWSPD. We thus define the normalized (discrete) path metric

$$\tilde{\ell}_p(x, y) := n^{\frac{p-1}{pd}} \ell_p(x, y). \quad (4)$$

The $n^{\frac{p-1}{pd}}$ normalization factor accounts for the fact that for $p > 1$, ℓ_p converges uniformly to 0 as $n \rightarrow \infty$. Note that the $1/p$ exponent in (1) and (3) is necessary to obtain a metric that is homogeneous. Moreover, as $p \rightarrow \infty$, \mathcal{L}_p is constant on regions of constant density, but \mathcal{L}_p^p is not. Indeed, consider a uniform distribution on $[0, 1]^d$, which has density $f = \mathbb{1}_{[0, 1]^d}$. Then for all $x, y \in [0, 1]^d$ and for all p , $\mathcal{L}_p^p(x, y) = \|x - y\|$. On the other hand, for all $x, y \in [0, 1]^d$, $\mathcal{L}_p(x, y) = \|x - y\|^{1/p} \rightarrow 1$ as $p \rightarrow \infty$, i.e. all points are equidistant in the limit $p \rightarrow \infty$. Thus the $1/p$ exponent in (1) and (3) is necessary to obtain an entirely density-based metric for large p .

In practice, computing PWSPDs in a sparse graph is preferable to computing them in a complete graph. It is thus natural to define PWSPDs *with respect to a subgraph \mathcal{H} of \mathcal{G}* .

Definition 1.3. *Let \mathcal{H} be any subgraph of \mathcal{G}_X^p . For $x, y \in X$, let $\mathcal{P}_{\mathcal{H}}(x, y)$ be the set of paths connecting x and y in \mathcal{H} . For $p \in [1, \infty)$ and for $x, y \in \mathcal{X}$, the (discrete) p -weighted shortest path distance (PWSPD) with respect to \mathcal{H} from x to y is:*

$$\ell_p^{\mathcal{H}}(x, y) = \min_{\pi = \{x_i\}_{i=1}^L \in \mathcal{P}_{\mathcal{H}}(x, y)} \left(\sum_{i=1}^{L-1} \|x_i - x_{i+1}\|^p \right)^{\frac{1}{p}}.$$

Clearly $\ell_p^{\mathcal{G}_X^p}(\cdot, \cdot) = \ell_p(\cdot, \cdot)$. In order to compute all-pairs PWSPDs in a complete graph with n nodes (i.e. $\ell_p(x_i, x_j)$ for all $x_i, x_j \in \mathcal{X}$), a direct application of Dijkstra's algorithm has complexity $O(n^3)$. If only the k -nearest neighbors (k NN) in PWSPD are desired, then a modified Dijkstra's algorithm with a pruning step allows all k NN in PWSPD to be computed in complexity $O(k^2 n \log(n) + C_d D n \log(n))$, where C_d is a constant that depends exponentially on the intrinsic dimensionality of the data [38]. When p is large, the PWSPDs derived from a complete graph are known in some cases to be the same as the PWSPDs derived from a k NN graph under particular scalings of $k \ll n$. This provides a significant computational advantage, since k NN graphs are much sparser, and reduces the complexity of computing all-pairs PWSPD to $O(kn^2)$ [33].

1.2 Summary of Contributions

This article develops new analyses, computational insights, and applications of PWSPDs, which may be summarized in three major contributions.

First, we establish that when $\frac{p}{d}$ is not too large, PWSPDs locally are density-rescaled Euclidean distances. This is particularly important when considering k NN in PWSPD, which is necessary when n is so large that computing all pairwise distances is impractical. We also develop related theory which clarifies the role of density in machine learning kernels more broadly. A range of machine learning kernels that normalize in order to mitigate or leverage differences in underlying density are considered and compared to PWSPD. Relatedly, we analyze how PWSPDs become increasingly influenced by the underlying density as $p \rightarrow \infty$. We also illustrate the role of density and benefits of PWSPDs compared to other data-dependent metrics on illustrative data sets.

Second, we develop near-optimal computational results on *spanners* for PWSPDs. Spanners for PWSPDs allow a computationally advantageous k NN graph to be considered when computing PWSPDs. Precise estimates on the number k of NN required, as a function of p and d , are developed. These results are proved generally for Riemannian manifolds, and provide an essential computational tool for the practical use of PWSPDs. Extending results of [26] and [16], we show that for all $p > 1$ one may take $k = O((4/(4^{1-1/p} - 1))^{d/2} \log(n))$, thus quantifying the dependence of k on p and improving the dependence of k on d , especially for large p . We demonstrate the tightness and usefulness of these spanner results in several simulations on large graphs, which in many cases suggest the near-optimality of our results with respect to p and d .

Third, we bound the convergence rate of PWSPD to its continuum limit using a percolation theory framework. Specifically, we develop bias and variance estimates by relating results on Euclidean first passage percolation to the PWSPD setting. Surprisingly, these results suggest that the variance of PWSPD is essentially independent of p , and depends on the intrinsic dimension d in complex ways. Numerical experiments not only verify our theoretical analyses, but also suggest several conjectures related to Euclidean first passage percolation that are of independent interest.

1.3 Notation

We shall use the notation in Table 1 consistently. We assume throughout that the data \mathcal{X} is drawn from a Riemannian data manifold (\mathcal{M}, g) . If $\mathcal{M} \subset \mathbb{R}^D$, we assume that it is isometrically embedded unless otherwise stated. Curvature assumptions on \mathcal{M} are introduced as needed.

NOTATION	DEFINITION
\mathcal{X}	A finite data set, $\mathcal{X} = \{x_i\}_{i=1}^n \subset \mathbb{R}^D$
$f(x)$	probability density function from which \mathcal{X} is drawn
\mathcal{M}	a Riemannian manifold
d	intrinsic dimension of data set \mathcal{X}
$\ell_p(x, y)$	discrete PWSPD, see (1)
$\mathcal{L}_p(x, y)$	continuum PWSPD, see (2)
$\bar{\ell}_p(x, y)$	rescaled version of $\ell_p(x, y)$, see (4)
$d(x, y)$	geodesic distance on manifold \mathcal{M}
$B_d(x, r)$	the geodesic ball of radius r , $\{y \in \mathcal{M} : d(x, y) \leq r\}$
$\ v\ _p$	the Euclidean p -norm of $v \in \mathbb{R}^D$, $\ v\ _p = (\sum_{i=1}^D v_i ^p)^{\frac{1}{p}}$
$\ v\ $	the Euclidean 2-norm
μ	percolation time constant
χ	percolation fluctuation exponent
\bar{A}	complement of the set A

Table 1: Notation used throughout the paper.

2 Local Analysis: Density and Kernels

Density-driven methods are commonly used for unsupervised and semisupervised learning [15, 22, 17, 42, 11, 6, 43]. Despite this popularity, the role of density is not completely clear in this context. Indeed, some methods seek to exploit variations in density while others mitigate it.

In this section, we explore the role that density plays in popular machine learning kernels, including those used in self-tuning spectral clustering and diffusion maps. We compare with the effect of density in ℓ_p -based kernels, and illustrate the primary advantages and disadvantages of these various approaches on some toy data sets.

2.1 Role of Density in Graph Laplacian Kernels

A large family of algorithms [7, 8, 47, 40, 51] view data points as the nodes of a graph, and define the corresponding edge weights via a kernel function. Given $\mathcal{X} \subset \mathbb{R}^D$, one first defines a weight matrix $W \in \mathbb{R}^{n \times n}$ and diagonal degree matrix $\text{Deg} \in \mathbb{R}^{n \times n}$ by $W_{ij} = \mathcal{K}(x_i, x_j)$ for some kernel \mathcal{K} , $\text{Deg}_{ii} = \sum_{j=1}^n W_{ij}$. A graph Laplacian L is then defined using W, Deg . Then, the K lowest

frequency eigenvectors of L , denoted ϕ_1, \dots, ϕ_K , define a K -dimensional spectral embedding of the data known as the *Laplacian eigenmaps* embedding by $x_i \mapsto (\phi_1(x_i), \phi_2(x_i), \dots, \phi_K(x_i))$, where $\phi_j(x_i) = (\phi_j)_i$. Commonly, a standard clustering algorithm such as K -means is then applied to the spectral embedding, and this procedure is known as *spectral clustering* (SC). In unnormalized SC, $L = \text{Deg} - W$, while in normalized SC either the random walk Laplacian $L_{\text{RW}} = \text{Deg}^{-1}L$ or the symmetric normalized Laplacian $L_{\text{SYM}} = \text{Deg}^{-1/2}L\text{Deg}^{-1/2}$ is used.

Many modifications of this general framework have been considered. Although SC is better able to handle irregularly shaped clusters than many traditional algorithms [4, 46], it is often unstable in the presence of low degree points and results are sensitive to the choice of scale parameter σ [51]. These shortcomings motivated [52] to apply SC with the *self-tuning kernel* $W_{ij} = \exp\left(-\frac{\|x_i - x_j\|^2}{\sigma_{i,k}\sigma_{j,k}}\right)$, where $\sigma_{i,k}$ is Euclidean distance of x_i to its k^{th} NN. To clarify how the data density influences this kernel, consider how $\sigma_{i,k}$ relates to the k NN density estimator at x_i :

$$f_n(x_i) := \frac{k}{\text{nvoll}(B_1^d)\sigma_{i,k}^d}. \quad (5)$$

It is known [35] that if $k = k(n)$ is such that $k(n) \rightarrow \infty$ while $k(n)/n \rightarrow 0$, then $f_n(x_i)$ is a consistent estimator of $f(x_i)$, as long as f is continuous and positive. Furthermore, if f is uniformly continuous and $k(n)/\log n \rightarrow \infty$ while $k(n)/n \rightarrow 0$, then $\sup_i |f_n(x_i) - f(x_i)| \rightarrow 0$ with probability 1 [20]. Although these results assume the density f is supported in \mathbb{R}^d , the density estimator (5) is consistent in the general case when f is supported on a d -dimensional Riemannian manifold $\mathcal{M} \subseteq \mathbb{R}^D$ [23] for $\log n \ll k(n) \ll n$. For such $k(n)$, $\sigma_{i,k} \rightarrow \epsilon_{n,d} f(x_i)^{-\frac{1}{d}}$ for some constant $\epsilon_{n,d}$ depending on n, d . Thus, for n large the kernel for self-tuning spectral clustering is approximately:

$$W_{ij} \approx \exp\left(-f(x_i)^{\frac{1}{d}} f(x_j)^{\frac{1}{d}} \frac{\|x_i - x_j\|^2}{\epsilon_{n,d}^2}\right). \quad (6)$$

Relative to a standard SC kernel, (6) weakens connections in high density regions and strengthens connections in low density regions.

Diffusion maps [18, 17] is a more general framework which reduces to SC for certain parameter choices. More specifically, [17] considered the family of kernels

$$W_{ij} = \frac{\exp(-\|x_i - x_j\|^2/\epsilon^2)}{d(x_i)^\alpha d(x_j)^\alpha}, \quad d(x_i) = \sum_{j=1}^n \exp(-\|x_i - x_j\|^2/\epsilon^2). \quad (7)$$

Since $d(x_i) \propto f(x_i) + O(\epsilon^2)$, $d(x_i)$ is a kernel density estimator of the density $f(x_i)$ [10] and, up to higher order terms,

$$W_{ij} \propto \frac{\exp(-\|x_i - x_j\|^2/\epsilon^2)}{f(x_i)^\alpha f(x_j)^\alpha}. \quad (8)$$

Note that f has an effect on the kernel similar to the self-tuning kernel (6): connections in high density regions are weakened, and connections in low density regions are strengthened. Let $L_{\text{RW}}^{\alpha,\epsilon}$ denote the discrete random walk Laplacian using the weights W_{ij} given in (7). The discrete operator $-L_{\text{RW}}^{\alpha,\epsilon}/\epsilon^2$ converges to the continuum Kolmogorov operator

$$\mathcal{L}\phi = \Delta\phi + (2 - 2\alpha)\nabla\phi \cdot \frac{\nabla f}{f}$$

as $n \rightarrow \infty, \epsilon \rightarrow 0^+$ [7, 17, 10]. When $\alpha = 0$ we recover standard spectral clustering; there is no density renormalization in the kernel but the limiting operator is density dependent. When $\alpha = 1$, $-L_{\text{RW}}^{1,\epsilon}/\epsilon^2 \rightarrow \Delta$; in this case the kernel is density dependent but the limiting operator is purely geometric, since the density term is eliminated.

2.2 Local Characterization of PWSPD-Based Kernels

While the kernels discussed in Section 2.1 compensate for discrepancies in density, PWSPD-based kernels strengthen connections through high-density regions and weaken connections through low-density regions. To illustrate more clearly the role of density in PWSPD-based kernels, we first show that locally the continuous PWSPD \mathcal{L}_p^p is well-approximated by the density-based *stretch* of Euclidean distance $d_{f,\text{euc}}(x, y) = \frac{\|x - y\|}{(f(x)f(y))^{\frac{p-1}{2d}}}$, as long as f does not vary too rapidly and \mathcal{M} does not curve too quickly. This is quantified in Lemma 2.2, which is then used to prove Theorem 2.3, which bounds the local deviation of \mathcal{L}_p , our metric of interest, from $d_{f,\text{euc}}^{1/p}$. Finally, Corollary 2.4 establishes that Gaussian kernels constructed with \mathcal{L}_p and $d_{f,\text{euc}}^{1/p}$ are locally similar. Throughout this section we assume $\mathcal{M} \in S(d, \kappa, \epsilon_0)$ as defined below.

Definition 2.1. *An isometrically embedded Riemannian manifold $\mathcal{M} \subset \mathbb{R}^D$ is an element of $S(d, \kappa, \epsilon_0)$ if it is compact with dimension d , $\text{vol}(\mathcal{M}) = 1$, and $d(x, y) \leq \|x - y\|(1 + \kappa\|x - y\|^2)$ for all $x, y \in \mathcal{M}$ such that $d(x, y) \leq \epsilon_0$, where $d(x, y)$ is the geodesic distance on \mathcal{M} .*

The condition $d(x, y) \leq \|x - y\|(1 + \kappa\|x - y\|^2)$ for all $x, y \in \mathcal{M}$ such that $d(x, y) \leq \epsilon_0$ is equivalent to an upper bound on the second fundamental form: $\|II_x\| \leq \kappa$ for all $x \in \mathcal{M}$ [3, 37].

Let $\mathcal{B}_{\mathcal{L}_p^p}(x, \epsilon)$ and $B_d(x, \epsilon)$ denote, respectively, the (closed) \mathcal{L}_p^p and geodesic balls centered at x of radius ϵ . Let $f_{\max} = \max_y\{f(y) : y \in \mathcal{M}\}$, $f_{\min} = \min_y\{f(y) : y \in \mathcal{M}\}$ be the global density maximum and minimum. We now define the following local quantities:

$$\begin{aligned} f_{\min}(x, \epsilon) &= \min_y \{f(y) : y \in B_d(x, \epsilon(1 + \kappa\epsilon^2))\}, \\ f_{\max}(x, \epsilon) &= \max_y \{f(y) : y \in \mathcal{B}_{\mathcal{L}_p^p}(x, \epsilon(1 + \kappa\epsilon^2)) / f_{\min}(x, \epsilon)^{\frac{p-1}{d}}\}. \end{aligned}$$

Let $\rho_{x,\epsilon} = f_{\max}(x, \epsilon)/f_{\min}(x, \epsilon)$, which characterizes the local discrepancy in density in a ball of radius $O(\epsilon)$ around the point x .

The following Lemma establishes that \mathcal{L}_p^p and $d_{f,\text{euc}}$ are locally equivalent, and that discrepancies depend on $(\rho_{x,\epsilon})^{\frac{p-1}{d}}$ and the curvature constant κ . We note similar estimates appear in [1] for the special case $p = 0$.

Lemma 2.2. *Let $\mathcal{M} \in S(d, \kappa, \epsilon_0)$. Then for all $y \in \mathcal{M}$ with $d(x, y) \leq \epsilon_0$ and $\|x - y\| \leq \epsilon$,*

$$\frac{1}{(\rho_{x,\epsilon})^{\frac{p-1}{d}}} d_{f,\text{euc}}(x, y) \leq \mathcal{L}_p^p(x, y) \leq (\rho_{x,\epsilon})^{\frac{p-1}{d}} (1 + \kappa\epsilon^2) d_{f,\text{euc}}(x, y). \quad (9)$$

Proof. Let $\gamma_1(t)$ be a path which achieves $d(x, y)$. Since $d(x, y) \leq \epsilon(1 + \kappa\epsilon^2)$, $f(\gamma_1(t)) \geq f_{\min}(x, \epsilon)$ for all t . Then:

$$\begin{aligned} \mathcal{L}_p^p(x, y) &\leq \int_0^1 \frac{1}{f(\gamma_1(t))^{\frac{p-1}{d}}} |\gamma_1'(t)| dt \\ &\leq \frac{d(x, y)}{f_{\min}(x, \epsilon)^{\frac{p-1}{d}}} \\ &\leq \frac{d(x, y)}{f_{\min}(x, \epsilon)^{\frac{p-1}{d}}} \frac{f_{\max}(x, \epsilon)^{\frac{p-1}{d}}}{(f(x)f(y))^{\frac{p-1}{2d}}} \\ &= (\rho_{x,\epsilon})^{\frac{p-1}{d}} \frac{d(x, y)}{(f(x)f(y))^{\frac{p-1}{2d}}} \end{aligned}$$

$$\begin{aligned}
&\leq (\rho_{x,\epsilon})^{\frac{p-1}{d}} \frac{\|x-y\|(1+\kappa\|x-y\|^2)}{(f(x)f(y))^{\frac{p-1}{2d}}} \\
&\leq (\rho_{x,\epsilon})^{\frac{p-1}{d}} (1+\kappa\epsilon^2) \frac{\|x-y\|}{(f(x)f(y))^{\frac{p-1}{2d}}} \\
&= (\rho_{x,\epsilon})^{\frac{p-1}{d}} (1+\kappa\epsilon^2) d_{f,\text{euc}}(x,y),
\end{aligned}$$

which proves the upper bound. Now let $\gamma_0(t)$ be a path achieving $\mathcal{L}_p^p(x,y)$; note that since $\mathcal{L}_p^p(x,y) \leq \frac{d(x,y)}{f_{\min}(x,\epsilon)^{\frac{p-1}{d}}}$, the path γ_0 is contained inside $\mathcal{B}_{\mathcal{L}_p^p}(x, \epsilon(1+\kappa\epsilon^2)/f_{\min}(x,\epsilon)^{\frac{p-1}{d}})$. Thus

$$\begin{aligned}
\mathcal{L}_p^p(x,y) &= \int_0^1 \frac{1}{f(\gamma_0(t))^{\frac{p-1}{d}}} |\gamma_0'(t)| dt \\
&\geq \frac{d(x,y)}{f_{\max}(x,\epsilon)^{\frac{p-1}{d}}} \\
&\geq \frac{d(x,y)}{f_{\max}(x,\epsilon)^{\frac{p-1}{d}}} \cdot \frac{f_{\min}(x,\epsilon)^{\frac{p-1}{d}}}{(f(x)f(y))^{\frac{p-1}{2d}}} \\
&= \frac{d(x,y)}{(\rho_{x,\epsilon})^{\frac{p-1}{d}} (f(x)f(y))^{\frac{p-1}{2d}}} \\
&\geq \frac{\|x-y\|}{(\rho_{x,\epsilon})^{\frac{p-1}{d}} (f(x)f(y))^{\frac{p-1}{2d}}} \\
&= \frac{1}{(\rho_{x,\epsilon})^{\frac{p-1}{d}}} d_{f,\text{euc}}(x,y),
\end{aligned}$$

which proves the lower bound. \square

Note that corresponding bounds in terms of geodesic distance follow easily from the definition of \mathcal{L}_p : $f_{\max}(x,\epsilon)^{-\frac{p-1}{d}} d(x,y) \leq \mathcal{L}_p^p(x,y) \leq f_{\min}(x,\epsilon)^{-\frac{p-1}{d}} d(x,y)$. Lemma 2.2 thus establishes that the metrics \mathcal{L}_p^p and $d_{f,\text{euc}}$ are locally equivalent when (i) $\rho_{x,\epsilon}$ is close to 1, (ii) $\frac{p-1}{d}$ is not too large, and (iii) κ is not too large. However, when $\frac{p-1}{d} \gg 1$, \mathcal{L}_p^p balls may become highly nonlocal in terms of geodesics.

The following Theorem establishes the local equivalence of \mathcal{L}_p and $d_{f,\text{Euc}}^{1/p}$ (and thus kernels constructed using these metrics). Assuming the density does not vary too quickly, Lemma 2.2 can be used to show that locally the difference between $d_{f,\text{euc}}^{1/p}$ and \mathcal{L}_p is small. Variations in density are controlled by requiring that f is L -Lipschitz with respect to geodesic distance, i.e. $|f(x) - f(y)| \leq Ld(x,y)$.

Theorem 2.3. *Assume $\mathcal{M} \in S(d,\kappa,\epsilon_0)$ and that f is a bounded, nonzero, L -Lipschitz density function on \mathcal{M} . Let*

$$\rho = \max_{x \in \mathcal{M}} \rho_{x,\epsilon}, \quad C_1 = \frac{L(\rho^{\frac{p-1}{d}} + 1)(p-1)}{f_{\min}^{1+\frac{p-1}{pd}} pd}, \quad C_2 = \frac{\kappa}{f_{\min}^{\frac{p-1}{pd}} p}.$$

Then for all $x,y \in \mathcal{M}$ such that $d(x,y) \leq \epsilon_0$ and $\|x-y\| \leq \epsilon$, $|\mathcal{L}_p(x,y) - d_{f,\text{euc}}^{1/p}(x,y)| \leq C_1 \epsilon^{1+\frac{1}{p}} + C_2 \epsilon^{2+\frac{1}{p}} + O(\epsilon^{3+\frac{1}{p}})$.

Proof. We first show that $\rho_{x,\epsilon}$ is close to 1. Let $y_1 \in \mathcal{B}_{\mathcal{L}_p^p}(x, \epsilon(1 + \kappa\epsilon^2)/f_{\min}(x, \epsilon)^{\frac{p-1}{d}})$ satisfy $f(y_1) = f_{\max}(x, \epsilon)$ and $y_2 \in B_d(x, \epsilon(1 + \kappa\epsilon^2))$ satisfy $f(y_2) = f_{\min}(x, \epsilon)$ (since these sets are compact, these points must exist). Then by the Lipschitz condition:

$$|\rho_{x,\epsilon} - 1| = \frac{|f(y_1) - f(y_2)|}{f(y_2)} \leq \frac{Ld(y_1, y_2)}{f(y_2)} \leq \frac{Ld(x, y_1) + Ld(x, y_2)}{f(y_2)}.$$

Let $\gamma_2(t)$ be a path achieving $\mathcal{L}_p^p(x, y_1)$. Note that

$$\frac{d(x, y_1)}{f_{\max}(x, \epsilon)^{\frac{p-1}{d}}} \leq \int_0^1 \frac{1}{f(\gamma_2(t))^{\frac{p-1}{d}}} |\gamma_2'(t)| dt = \mathcal{L}_p^p(x, y_1) \leq \frac{\epsilon(1 + \kappa\epsilon^2)}{f_{\min}(x, \epsilon)^{\frac{p-1}{d}}}$$

so that $d(x, y_1) \leq \rho_{x,\epsilon}^{\frac{p-1}{d}} \epsilon(1 + \kappa\epsilon^2)$, $d(x, y_2) \leq \epsilon(1 + \kappa\epsilon^2)$. We thus obtain

$$\rho_{x,\epsilon} \leq 1 + L \left(\frac{\rho_{x,\epsilon}^{\frac{p-1}{d}} + 1}{f_{\min}(x, \epsilon)} \right) \epsilon(1 + \kappa\epsilon^2). \quad (10)$$

Letting $C_{x,\epsilon} = L(\rho_{x,\epsilon}^{\frac{p-1}{d}} + 1)/f_{\min}(x, \epsilon)$, Taylor expanding around $\epsilon = 0$ and (10) give $\rho_{x,\epsilon}^{\frac{p-1}{d}} \leq (1 + C_{x,\epsilon}\epsilon(1 + \kappa\epsilon^2))^{\frac{p-1}{pd}} = 1 + C_{x,\epsilon} \frac{(p-1)}{pd} \epsilon + O(\epsilon^3)$. Applying Lemma 2.2 yields $(\rho_{x,\epsilon})^{-\frac{p-1}{pd}} d_{f,\text{euc}}^{1/p}(x, y) \leq \mathcal{L}_p(x, y) \leq (\rho_{x,\epsilon})^{\frac{p-1}{pd}} (1 + \kappa\epsilon^2)^{\frac{1}{p}} d_{f,\text{euc}}^{1/p}(x, y)$, which gives

$$\frac{d_{f,\text{euc}}^{1/p}(x, y)}{\left(1 + C_{x,\epsilon} \frac{(p-1)}{pd} \epsilon + O(\epsilon^3)\right)} \leq \mathcal{L}_p(x, y) \leq \left(1 + C_{x,\epsilon} \frac{(p-1)}{pd} \epsilon + O(\epsilon^3)\right) \left(1 + \frac{\kappa}{p} \epsilon^2 + O(\epsilon^4)\right) d_{f,\text{euc}}^{1/p}(x, y).$$

Rewriting the above yields:

$$\left(1 - C_{x,\epsilon} \frac{(p-1)}{pd} \epsilon - \frac{\kappa}{p} \epsilon^2 + O(\epsilon^3)\right) \mathcal{L}_p(x, y) \leq d_{f,\text{euc}}^{1/p}(x, y) \leq \mathcal{L}_p(x, y) \left(1 + C_{x,\epsilon} \frac{(p-1)}{pd} \epsilon + O(\epsilon^3)\right).$$

We thus obtain

$$\begin{aligned} \left| \mathcal{L}_p(x, y) - d_{f,\text{euc}}^{1/p}(x, y) \right| &\leq \left(C_{x,\epsilon} \frac{(p-1)}{pd} \epsilon + \frac{\kappa}{p} \epsilon^2 + O(\epsilon^3) \right) \mathcal{L}_p(x, y) \\ &\leq \left(C_{x,\epsilon} \frac{(p-1)}{pd} \epsilon + \frac{\kappa}{p} \epsilon^2 + O(\epsilon^3) \right) \frac{\epsilon^{\frac{1}{p}} (1 + \kappa\epsilon^2)^{\frac{1}{p}}}{f_{\min}(x, \epsilon)^{\frac{p-1}{pd}}} \\ &= \left(\frac{C_{x,\epsilon}}{f_{\min}(x, \epsilon)^{\frac{p-1}{pd}}} \frac{(p-1)}{pd} \epsilon^{1+\frac{1}{p}} + \frac{\kappa}{pf_{\min}(x, \epsilon)^{\frac{p-1}{pd}}} \epsilon^{2+\frac{1}{p}} + O(\epsilon^{3+\frac{1}{p}}) \right). \end{aligned}$$

□

Note the coefficient C_1 increases exponentially in p ; thus the equivalence between \mathcal{L}_p and $d_{f,\text{Euc}}^{1/p}$ is weaker for large p . We also emphasize that in a Euclidean ball of radius ϵ , the metric \mathcal{L}_p scales like $\epsilon^{\frac{1}{p}}$; Theorem 2.3 thus guarantees that the relative error of approximating \mathcal{L}_p with $d_{f,\text{Euc}}^{1/p}$ is $O(\epsilon)$.

When the metric \mathcal{L}_p is locally well-approximated by the metric $d_{f,\text{euc}}^{1/p}$, the kernels constructed from these two metrics are also locally similar. The following Corollary makes this precise for Gaussian kernels. Let $h_a(x) = \exp(-x^{2a})$ so that $h_1(x)$ is a Gaussian kernel, and note that $h_1\left(\frac{\mathcal{L}_p}{\epsilon^{1/p}}\right) = h_{\frac{1}{p}}\left(\frac{\mathcal{L}_p}{\epsilon}\right)$.

Corollary 2.4. Under the assumptions and notation of Theorem 2.3, for $\tilde{C}_i = C_i/f_{\min}^{\frac{p-1}{pd}}$,

$$\left| \frac{h_{\frac{1}{p}}(\mathcal{L}_p^p(x, y)/\epsilon) - h_{\frac{1}{p}}(d_{f, \text{Euc}}(x, y)/\epsilon)}{h_{\frac{1}{p}}(\mathcal{L}_p^p(x, y)/\epsilon)} \right| \leq \tilde{C}_1\epsilon + \left(\tilde{C}_2 + \frac{1}{2}\tilde{C}_1^2 \right) \epsilon^2 + O(\epsilon^3).$$

Proof. First note that

$$\begin{aligned} \left| \mathcal{L}_p^2(x, y) - d_{f, \text{Euc}}^{2/p}(x, y) \right| &= \left| \left(\mathcal{L}_p(x, y) - d_{f, \text{Euc}}^{1/p}(x, y) \right) \left(\mathcal{L}_p(x, y) + d_{f, \text{Euc}}^{1/p}(x, y) \right) \right| \\ &\leq \left| \left(C_1\epsilon^{1+\frac{1}{p}} + C_2\epsilon^{2+\frac{1}{p}} + O(\epsilon^{3+\frac{1}{p}}) \right) \frac{\epsilon^{1/p}(1 + O(\epsilon^2))}{f_{\min}^{\frac{p-1}{pd}}} \right| \\ &= \tilde{C}_1\epsilon^{1+2/p} + \tilde{C}_2\epsilon^{2+2/p} + O(\epsilon^{3+2/p}). \end{aligned}$$

Thus

$$\begin{aligned} \left| \frac{h_{\frac{1}{p}}(\mathcal{L}_p^p(x, y)/\epsilon) - h_{\frac{1}{p}}(d_{f, \text{Euc}}(x, y)/\epsilon)}{h_{\frac{1}{p}}(\mathcal{L}_p^p(x, y)/\epsilon)} \right| &= \left| 1 - \exp \left(-\frac{d_{f, \text{Euc}}^{2/p}(x, y)}{\epsilon^{2/p}} + \frac{\mathcal{L}_p^2(x, y)}{\epsilon^{2/p}} \right) \right| \\ &= \left| 1 - \exp(\pm[\tilde{C}_1\epsilon + \tilde{C}_2\epsilon^2 + O(\epsilon^3)]) \right| \\ &\leq \tilde{C}_1\epsilon + \left(\tilde{C}_2 + \frac{1}{2}\tilde{C}_1^2 \right) \epsilon^2 + O(\epsilon^3). \end{aligned}$$

□

When $p-1$ is not too large relative to d , a kernel constructed with \mathcal{L}_p is locally well-approximated by a kernel constructed with $d_{f, \text{Euc}}^{1/p}$. Thus, in a Euclidean ball of radius ϵ , we may think of the Gaussian \mathcal{L}_p kernel as:

$$h_1 \left(\frac{\mathcal{L}_p(x_i, x_j)}{\epsilon^{1/p}} \right) \approx h_{\frac{1}{p}} \left(\frac{\|x_i - x_j\|}{\epsilon(f(x_i)f(x_j))^{\frac{p-1}{2d}}} \right).$$

Density plays a different role in this kernel compared with the kernels of Section 2.1. This kernel strengthens connections in high density regions, and weakens connections in low density regions.

We remark that the $\frac{1}{p}$ -power in Definition 1.2 has a large impact, in that \mathcal{L}_p -based and \mathcal{L}_p^p -based kernels have very different properties. More specifically, $h_1(\mathcal{L}_p^p/\epsilon)$ is a local kernel as defined in [10], so it is sufficient to analyze the kernel locally. However $h_1(\mathcal{L}_p/\epsilon^{1/p})$ is a non-local kernel, so that non-trivial connections between distant points are possible. The analysis in this section thus establishes the global equivalence of $h_1(\mathcal{L}_p^p/\epsilon)$ and $h_1(d_{f, \text{Euc}}/\epsilon)$ (when p is not too large relative to d) but only the local equivalence of $h_{\frac{1}{p}}(\mathcal{L}_p^p/\epsilon)$ and $h_{\frac{1}{p}}(d_{f, \text{Euc}}/\epsilon)$.

2.3 The Role of p : Examples

This subsection illustrates the useful properties of PWSPDs and the role of p on three synthetic data sets in \mathbb{R}^2 : (1) *Two Rings* data, consisting of two non-convex clusters that are well-separated by a low-density region; (2) *Long Bottleneck* data, consisting of two isotropic clusters with a density gap connected by a long, thin bottleneck; (3) *Short Bottleneck* data, where two elongated clusters are connected by a short bottleneck. The data sets are shown in Figures 1, 2, and 3, respectively.

Comparisons are made between several methods of spectral embedding: Euclidean spectral clustering (SC); Euclidean SC with self-tuning (ST); Euclidean SC with the diffusion maps normalization (DMN); and PWSPD SC with different choices of p . All methods besides self-tuning SC used a scaling parameter equal to the 15th percentile of all pairwise distances when sorted from smallest to largest. The self-tuning kernel determined the scaling parameter using the distance to the 10th nearest neighbor.

To evaluate how p impacts the clusterability of the PWSPD spectral embedding, we run K -means for a range of p values on the spectral embedding $x_i \mapsto \phi_2(x_i)$, where ϕ_2 is the second lowest-frequency eigenvector of the PWSPD Laplacian. The results in terms of overall accuracy of the clustering (ratio of points correctly labeled after alignment with ground truth labels) as a function of p are in (h) of Figures 1, 2, and 3. We note that PWSPDs with $p = 1$ is exactly the same as Euclidean distances, because the graph underlying the PWSPD calculation is complete. We also show the embeddings $x_i \mapsto (\phi_2(x_i), \phi_3(x_i))$, where ϕ_2, ϕ_3 are the second and third lowest-frequency Laplacian eigenvectors for each of the comparison methods.

We see that when density separates the data clearly, as in the Two Rings data, large p gives strong clustering results, while small p may fail. On the other hand, if the clusters are compact but connected by a thin, high-density bridge as in the Long Bottleneck data, small p works well while large p fails. In between these cases, in the Short Bottleneck data, neither density nor geometry alone are able to capture the cluster structure, and the optimal p is a middle ground $1 < p \ll \infty$.

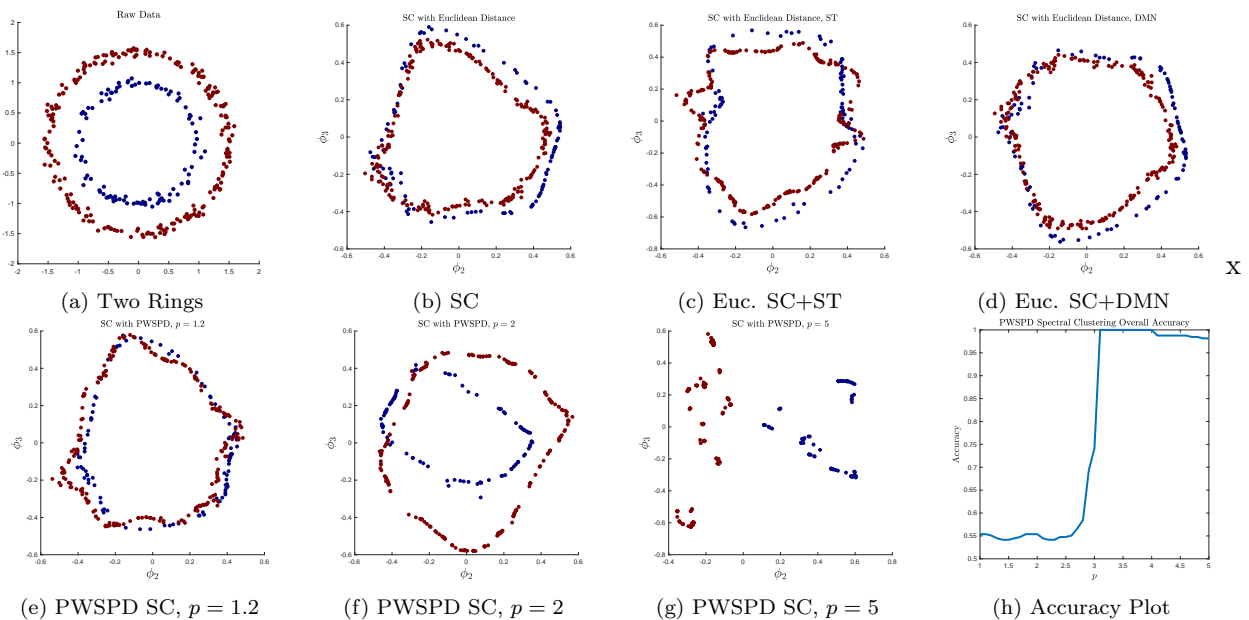


Figure 1: The *Two Rings* dataset consists of two clusters that are non-convex, but well-separated by a region of low density. We see that embedding with the principal eigenfunctions of a PWSPD Laplacian works well when the density weighting parameter $p > 3$. This is because the underlying cluster structure is essentially density-driven.

3 Spanners for PWSPD

Recall the definition of $\ell_p^{\mathcal{H}}(\cdot, \cdot)$ given in Definition 1.3. Clearly, $\ell_p(x, y) \leq \ell_p^{\mathcal{H}}(x, y)$ for all \mathcal{H} and all $x, y \in \mathcal{X}$, as any path in \mathcal{H} is automatically a path in $\mathcal{G}_{\mathcal{X}}^p$. Surprisingly, it has been shown that if \mathcal{H} is taken to be the k NN graph, for appropriate k , then we in fact have equality: $\ell_p(x, y) = \ell_p^{\mathcal{H}}(x, y)$ for all $x, y \in \mathcal{X}$, at least with high probability. Recall that the k NN graph, which we shall denote

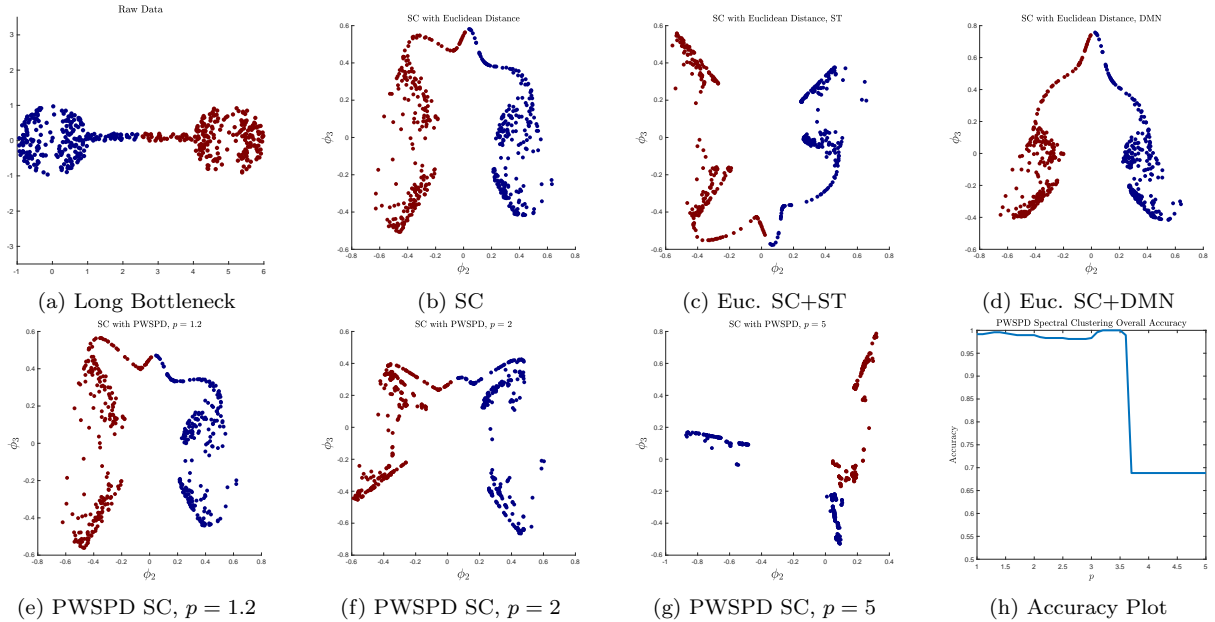


Figure 2: The *Long Bottleneck* dataset consists of two clusters that are convex, but connected by a thin bottleneck. We see that embedding with the principal eigenfunctions of a PWSPD Laplacian works well when the density weighting parameter $p \leq 3.5$, but fails for larger values of p . This is because the underlying cluster structure is essentially driven by the geometry of the data, while the density is misleading for clustering.

$\mathcal{G}_{\mathcal{X}}^{p,k}$, is the subgraph of $\mathcal{G}_{\mathcal{X}}^p$ that only retains edges $\{x_i, x_j\}$ when x_i is amongst the k nearest points to x_j in the Euclidean metric, or vice versa. It is useful to formalize the equality of distances with the following definition:

Definition 3.1. A subgraph $\mathcal{H} \subset \mathcal{G}_{\mathcal{X}}^p$ is a 1-spanner if for all $x, y \in \mathcal{X}$, $\ell_p(x, y) = \ell_{\mathcal{H}}(x, y)$.

The work of [26] and [16] independently show that $\mathcal{G}_{\mathcal{X}}^{p,k}$ is a 1-spanner of $\mathcal{G}_{\mathcal{X}}^p$, for appropriate values of k and p and in particular settings. Specifically, [26] shows that for any $1 < p < \infty$, $\mathcal{G}_{\mathcal{X}}^{p,k}$ is a 1-spanner of $\mathcal{G}_{\mathcal{X}}^p$ for $k = O(\theta_{d,p} \log(n))$. One can deduce that $\theta_{d,p} \geq 2^{d+1} 3^d d^{d/2}$, but the exact dependence on p is unclear. Moreover, their proof only holds when \mathcal{M} is the image of an open set $U \subset \mathbb{R}^d$. A different approach is used in [16], which shows that $\mathcal{G}_{\mathcal{X}}^{p,k}$ is a 1-spanner of $\mathcal{G}_{\mathcal{X}}^p$ for data sampled from an arbitrary data manifold \mathcal{M} if $k = O(2^d \log(n))$ and $p \geq 2$.

In this section we prove that the k NN graph is a 1-spanner, for arbitrary data manifold, for $1 < p < \infty$ with improved dependence of k on d and explicit dependence of k on p . We first consider the more common case where $\mathcal{M} \subset \mathbb{R}^D$ is isometrically embedded (see Section 3.1). In Section 3.2 we then consider the case where \mathcal{M} is not necessarily isometrically embedded. Finally, in Section 3.3 we verify the dependence of k on n, d and p experimentally. Before proceeding, let us introduce some further terminology:

Definition 3.2. An edge $\{x, y\}$ in $\mathcal{G}_{\mathcal{X}}^p$ is critical if it is the shortest path from x to y in $\mathcal{G}_{\mathcal{X}}^p$.

As noted in [16], critical edges give us a sufficient condition for 1-spanners:

Lemma 3.3. $\mathcal{H} \subset \mathcal{G}_{\mathcal{X}}^p$ is a 1-spanner if it contains every critical edge of $\mathcal{G}_{\mathcal{X}}^p$.

3.1 PWSPD Spanners: \mathcal{M} is isometrically embedded

The key ingredient in our proof is what we call a p -elongated set, which generalizes the role of spheres in the proof of Theorem 1.3 in [16].

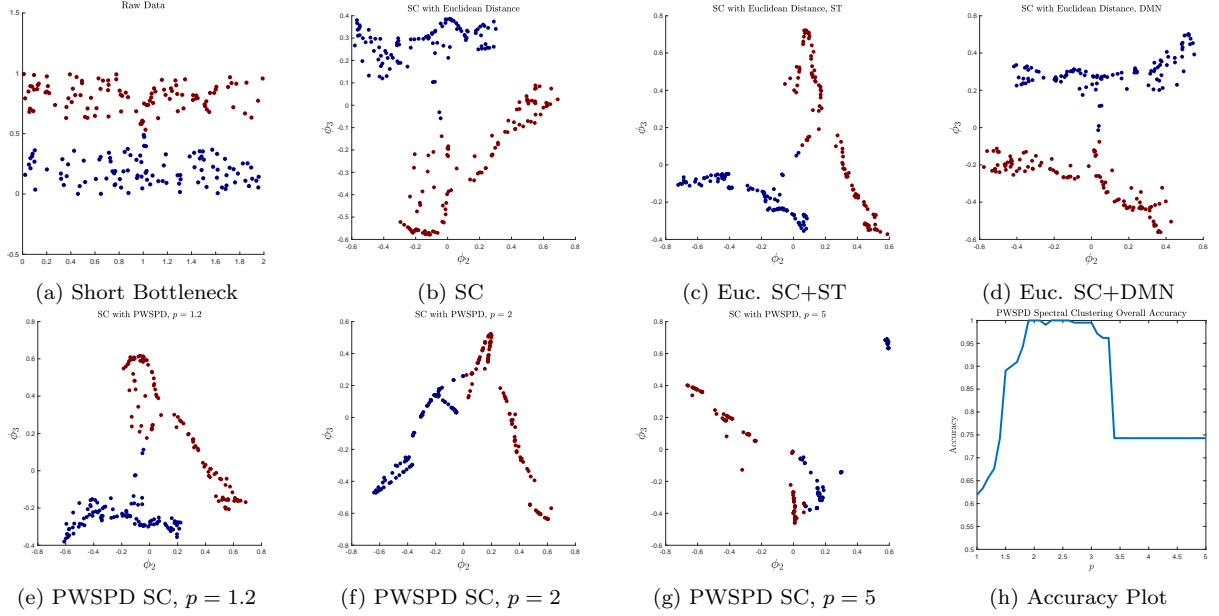


Figure 3: The *Short Bottleneck* dataset consists of two elongated clusters that are connected by a short bridge. We see that embedding with the principal eigenfunctions of a PWSPD Laplacian works well when the density weighting parameter $1.8 \leq p \leq 3$. This is because the underlying cluster structure is not driven entirely by geometry (so p near 1 fails), but also is not driven purely by density (so large p fails). Indeed, this is an example where a good metric balances geometry and density.

Definition 3.4. For any $x, y \in \mathbb{R}^d$ and $\alpha \in (0, 1]$, the p -elongated set associated to x, y is

$$\mathcal{D}_{\alpha,p}(x, y) = \left\{ z \in \mathbb{R}^d : \|x - z\|^p + \|y - z\|^p \leq \alpha \|x - y\|^p \right\}.$$

Note that $\mathcal{D}_{1,p}(x, y)$ is precisely the set of points, z , such that the two-hop path, $x \rightarrow z \rightarrow y$, is ℓ_p -shorter than the one-hop path, $x \rightarrow y$. $\mathcal{D}_{\alpha,2}(x, y)$ is a ball with diameter $\alpha \|x - y\|$, while for other values of p the $\mathcal{D}_{\alpha,p}(x, y)$ are shaped like an American football.

Lemma 3.5. $\mathcal{D}_{\alpha,p}(x, y)$ contains a ball of radius $\|x - y\| \sqrt{\frac{\alpha^{2/p} - 1}{4^{1/p}} - \frac{1}{4}}$ centered at $x_M = \frac{x+y}{2}$.

Proof. Let $s := \|x - y\|$ and choose a coordinate system $x^{(1)}, \dots, x^{(n)}$ such that with respect to these coordinates $y = (-s/2, 0, \dots, 0)$ and $x = (s/2, 0, \dots, 0)$. The region $\mathcal{D}_{\alpha,p}(x, y)$ is now the interior of:

$$\left(\left(x^{(1)} + \frac{s}{2} \right)^2 + (x^{(2)})^2 + \dots + (x^{(n)})^2 \right)^{p/2} + \left(\left(x^{(1)} - \frac{s}{2} \right)^2 + (x^{(2)})^2 + \dots + (x^{(n)})^2 \right)^{p/2} = \alpha s^p.$$

In spherical coordinates the boundary of this region may be expressed as:

$$(r^2 + sr \cos \phi_1 + s^2/4)^{p/2} + (r^2 - sr \cos \phi_1 + s^2/4)^{p/2} = \alpha s^p \quad (11)$$

where $(x^{(1)})^2 + (x^{(2)})^2 + \dots + (x^{(n)})^2 = r^2$ and $x_1 = r \cos \phi_1$. Now define $r = h(\phi_1)$ as the unique positive solution of (11) for a fixed ϕ_1 , i.e. we view r as a function of ϕ_1 . Implicitly differentiating in ϕ_1 yields

$$\frac{p}{2} \left(r^2 + sr \cos(\phi_1) + \frac{s^2}{4} \right)^{\frac{p}{2}-1} \left(2r \frac{dr}{d\phi_1} - sr \sin(\phi_1) + s \cos(\phi_1) \frac{dr}{d\phi_1} \right)$$

$$+\frac{p}{2} \left(r^2 - sr \cos(\phi_1) + \frac{s^2}{4} \right)^{\frac{p}{2}-1} \left(2r \frac{dr}{d\phi_1} + sr \sin(\phi_1) - s \cos(\phi_1) \frac{dr}{d\phi_1} \right) = 0$$

Solving for $\frac{dr}{d\phi_1}$ and setting the result to 0 yields

$$\underbrace{\left[\left(r^2 + sr \cos(\phi_1) + \frac{s^2}{4} \right)^{\frac{p-2}{2}} - \left(r^2 - sr \cos(\phi_1) + \frac{s^2}{4} \right)^{\frac{p-2}{2}} \right]}_{:=\text{(I)}} \underbrace{\sin(\phi_1)}_{:=\text{(II)}} = 0.$$

Thus we obtain two solutions to $\frac{dr}{d\phi_1} = 0$:

$$\text{(I)} = 0 \Rightarrow \cos(\phi_1) = 0 \Rightarrow \phi_1 = \frac{\pi}{2} \quad (\text{minimum})$$

$$\text{(II)} = 0 \Rightarrow \sin(\phi_1) = 0 \Rightarrow \phi_1 = 0 \quad (\text{maximum})$$

So we can see that the minimal radius occurs when $\phi_1 = \frac{\pi}{2}$. The minimal radius is obtained by substituting $\phi_1 = \frac{\pi}{2}$ into (11) and solving for r , which yields:

$$r = s \sqrt{\frac{\alpha^{2/p}}{4^{1/p}} - \frac{1}{4}} = \|x - y\| \sqrt{\frac{\alpha^{2/p}}{4^{1/p}} - \frac{1}{4}}.$$

By construction, the ball of radius r is contained in $\mathcal{D}_{\alpha,p}(x_i, x_j)$, as desired. \square

A similar claim is made in [26] in the case $\alpha = 1$, but crucially does not quantify the dependence of the radius of this ball on p . Before proceeding, we introduce a regularity assumption:

Definition 3.6. A set $\mathcal{M} \subset \mathbb{R}^D$ is an element of $V(d, \kappa, \epsilon_0)$ for $\kappa \geq 1$ and $\epsilon_0 > 0$ if it is connected and for all $x \in \mathcal{M}$, $\epsilon \in (0, \epsilon_0)$ we have: $\kappa^{-1} \epsilon^d \leq \text{vol}(\mathcal{M} \cap B(x, \epsilon)) / \text{vol}(B(0, 1)) \leq \kappa \epsilon^d$.

Theorem 3.7. Let $\mathcal{M} \in V(d, \kappa, \epsilon_0)$ be compact and convex. Let $\mathcal{X} = \{x_i\}_{i=1}^n$ be drawn i.i.d. from \mathcal{M} according to a probability distribution f . For n sufficiently large, if $k \geq 1 + \kappa^2 \frac{3f_{\max}}{f_{\min}} \left(\frac{4}{4^{1-1/p}-1} \right)^{d/2} \log(n)$ then $\mathcal{G}_{\mathcal{X}}^{p,k}$ is a 1-spanner of $\mathcal{G}_{\mathcal{X}}^p$ with probability at least $1 - 1/n$.

For $p = 2$ we attain $k = O(2^d \log(n))$ as in [16]. For large p we get $k \approx O\left(\left(\frac{4}{3}\right)^{d/2} \log(n)\right)$, thus improving the dependence of k on d given in [26, 16]. Our proof generalizes the approach of [16].

Proof. In light of Lemma 3.3, we shall prove that with probability at least $1 - 1/n$, $\mathcal{G}_{\mathcal{X}}^{p,k}$ contains every critical edge of $\mathcal{G}_{\mathcal{X}}^p$. Equivalently, we show that every edge of $\mathcal{G}_{\mathcal{X}}^p$ that is not contained in $\mathcal{G}_{\mathcal{X}}^{p,k}$ is not critical.

Pick any point in \mathcal{X} . Without loss of generality, assume that this point is x_1 . Let x_{i_1}, \dots, x_{i_k} denote the k NNs of x_1 , ordered randomly, and let r_k denote the distance to the k^{th} NN. Because \mathcal{M} is compact, $r_k \rightarrow 0$ as $n \rightarrow \infty$. As long as $\|x_1 - x_{i_j}\| < r_k$:

$$\text{for all } U \subset B(x_1, r_k), \mathbb{P}[x_{i_j} \in U \mid x_{i_j} \in B(x_1, r_k)] = \int_{U \cap \mathcal{M}} f(x) / \int_{B(x_1, r_k) \cap \mathcal{M}} f(x). \quad (12)$$

Let x_i be any point which is not a k NN of x_1 . We claim that the edge $\{x_1, x_i\}$ is *not* critical, with high probability. Define \bar{x}_i to be the projection of x_i onto the boundary of $B(x_1, r_k)$. Consider the p -elongated set $\mathcal{D}_{1,p}(x_1, \bar{x}_i)$ as in Definition 3.4. If there is an $x_{i_j} \in \mathcal{D}_{1,p}(x_1, \bar{x}_i)$ then $\|x_1 -$

$\|x_{i_j}\|^p + \|x_{i_j} - \bar{x}_i\|^p \leq \|x_1 - \bar{x}_i\|^p \leq \|x_1 - x_i\|^p$ and hence the two-hop path $x_1 \rightarrow x_{i_j} \rightarrow x_i$ is p -weighted shorter than the direct path $x_1 \rightarrow x_i$, or at least the same length. Hence, $\{x_1, x_i\}$ is not critical. Let us show that such an x_{i_j} exists, with high probability. Because \mathcal{M} is convex, the midpoint $x_M = (x_1 + \bar{x}_i)/2 \in \mathcal{M}$. Let $r_{1,p} := r_k \sqrt{1/4^{1/p} - 1/4}$; from Lemma 3.5, we get that $B(x_M, r_{1,p}) \subset \mathcal{D}_{1,p}(x_1, \bar{x}_i)$. Because $\mathcal{M} \in V(d, \kappa, \epsilon_0)$:

$$\begin{aligned} \text{vol}(B(x_M, r_{1,p}) \cap \mathcal{M}) &\geq \kappa^{-1} \text{vol}(B(0, 1)) r_{1,p}^d = \kappa^{-1} \text{vol}(B(0, 1)) r_k^d \left(\frac{1}{4^{1/p}} - \frac{1}{4} \right)^{d/2}, \\ \text{vol}(B(x_1, r_k) \cap \mathcal{M}) &\leq \kappa \text{vol}(B(x_1, r_k)) = \kappa \text{vol}(B(0, 1)) r_k^d \end{aligned}$$

as long as n is large enough such that $r_k \leq \epsilon_0$. From (12):

$$\begin{aligned} \mathbb{P}[x_{i_j} \in \mathcal{D}_{1,p}(x_1, \bar{x}_i) \mid x_{i_j} \in B(x_1, r_k)] &= \frac{\int_{\mathcal{D}_{1,p}(x_1, \bar{x}_i) \cap \mathcal{M}} f(x)}{\int_{B(x_1, r_k) \cap \mathcal{M}} f(x)} \\ &\geq \frac{f_{\min} \text{vol}(\mathcal{D}_{1,p}(x_1, \bar{x}_i) \cap \mathcal{M})}{f_{\max} \text{vol}(B(x_1, r_k) \cap \mathcal{M})} \\ &\geq \frac{f_{\min} \kappa^{-1} \text{vol}(B(0, 1)) r_k^d \left(\frac{1}{4^{1/p}} - \frac{1}{4} \right)^{d/2}}{f_{\max} \kappa \text{vol}(B(0, 1)) r_k^d} \\ &= \kappa^{-2} \frac{f_{\min}}{f_{\max}} \left(\frac{1}{4^{1/p}} - \frac{1}{4} \right)^{d/2} =: \kappa^{-2} \varepsilon_{d,p,f}. \end{aligned}$$

Because the x_{i_j} are all independently drawn:

$$\mathbb{P}[\nexists j \text{ with } x_{i_j} \in \mathcal{D}_{1,p}(x_1, \bar{x}_i)] = \prod_{j=1}^{k-1} \mathbb{P}[x_{i_j} \notin \mathcal{D}_{1,p}(x_1, \bar{x}_i)] \leq (1 - \kappa^{-2} \varepsilon_{d,p,f})^{k-1}.$$

For any $k \geq 1 + \log(n^3)/(-\log(1 - \kappa^{-2} \varepsilon_{d,p,f}))$:

$$\mathbb{P}[\{x_1, x_i\} \text{ is critical}] \leq \mathbb{P}[\nexists j \in \{2, \dots, k\} \text{ with } x_{i_j} \in \mathcal{D}_{1,p}(x_1, \bar{x}_i)] \leq \frac{1}{n^3}.$$

Because x_1 and x_i were arbitrary, for any x_i, x_j which are not k NNs: $\mathbb{P}[\{x_i, x_j\} \text{ is critical}] \leq 1/n^3$. By a union bound,

$$\begin{aligned} &\mathbb{P}[\exists x_i, x_j \text{ not } k\text{NNs but } \{x_i, x_j\} \text{ is critical}] \\ &\leq \mathbb{P}[\text{All } \{x_i, x_j\} \text{ are critical where } x_i, x_j \text{ are not } k\text{NNs}] \\ &\leq n^2 \mathbb{P}[\{x_i, x_j\} \text{ is critical}] = \frac{1}{n}, \end{aligned}$$

and so $\mathcal{G}_{\chi}^{p,k}$ is a 1-spanner with probability $1 - 1/n$ as claimed. Note that:

$$1 + \kappa^2 \frac{3f_{\max}}{f_{\min}} \left(\frac{4}{4^{1-1/p} - 1} \right)^{d/2} \log(n) \geq 1 + 3 \log(n)/(-\log(1 - \kappa^{-2} \varepsilon_{d,p,f}))$$

by unpacking the definition of $\varepsilon_{d,p,f}$ and using $\log\left(\frac{1}{1 - \kappa^{-2} \varepsilon_{d,p,f}}\right) \geq \kappa^{-2} \varepsilon_{d,p,f}$. \square

3.2 PWSPD Spanners: Intrinsic Path Distance

In this section we assume that \mathcal{M} is a compact Riemannian manifold with metric g , but we *do not* assume that \mathcal{M} is isometrically embedded in \mathbb{R}^D . We consider an *intrinsic* version of PWSPD,

$$\ell_{\mathcal{M},p}(x, y) = \left(\min_{\pi=\{x_i\}_{i=1}^L} \sum_{i=1}^{L-1} d(x_i, x_{i+1})^p \right)^{1/p},$$

and prove a result analogous to Theorem 3.7. Let $\mathcal{G}_{\mathcal{M},\mathcal{X}}^p$ denote the complete graph on \mathcal{X} with edge weights $d(x_i, x_j)^p$ while $\mathcal{G}_{\mathcal{M},\mathcal{X}}^{p,k}$ shall denote the k NN subgraph of $\mathcal{G}_{\mathcal{M},\mathcal{X}}^p$. Note that we are assuming that the geodesic distance $d(\cdot, \cdot)$ is known, which is not usually the case in data science. However, this situation can occur when \mathcal{X} is presented as a subset of \mathbb{R}^D , but one wishes to analyze \mathcal{X} with an exotic metric that is not $\|\cdot\|$. For example, if each $x_i \in \mathcal{X}$ represents an $M \times N$ image, it might be more appropriate to use a Wasserstein distance instead of the Euclidean distance. Let us first establish some notation. For precise definitions of terms in italics, we refer the reader to [41].

- For any $v, w \in T_x\mathcal{M}$, $R_x(v, w)$ denotes the *Riemannian curvature* while $K_x(v, w)$ denotes the *sectional curvature*. In this notation, $R_x(v, w)$ is a matrix while $K_x(v, w)$ is a scalar. These notions of curvature are related:

$$\langle R_x(w, v)w, v \rangle = K_x(v, w) (\|v\|^2\|w\|^2 - \langle v, w \rangle). \quad (13)$$

We shall drop the “ x ” in the subscript when it is clear from context. Let K_{\min} be such that $K_x(v, w) \geq K_{\min}$ for all $x \in \mathcal{M}$ and $v, w \in T_x\mathcal{M}$. Because \mathcal{M} is compact, such a K_{\min} exists. Similarly, S_x denotes the *scalar curvature* and $S_{\min} = \min_{x \in \mathcal{M}} S_x$ while $S_{\max} = \max_{x \in \mathcal{M}} S_x$.

- For $r > 0$, define $V_{\min}(r) := \min_{x \in \mathcal{M}} \text{vol}(B_d(x, r))$, $V_{\max}(r) = \max_{x \in \mathcal{M}} \text{vol}(B_d(x, r))$. Both quantities can be expressed as a Taylor series in r , with coefficients depending on the curvature of \mathcal{M} [25]:

$$V_{\min}(r) = \left(1 - \frac{S_{\max}}{6(d+2)}r^2 + O(r^4) \right) \text{vol}(B(0, 1))r^d, \quad (14)$$

$$V_{\max}(r) = \left(1 - \frac{S_{\min}}{6(d+2)}r^2 + O(r^4) \right) \text{vol}(B(0, 1))r^d. \quad (15)$$

- For any $x \in \mathcal{M}$, $\exp_x : T_x\mathcal{M} \rightarrow \mathcal{M}$ denotes the *exponential map*. By construction, $d(x, \exp_x(v)) = g_x(v, v)$. The exponential map is used to construct *normal coordinates*.
- The *injectivity radius* at x is denoted by $\text{inj}(x)$, while $\text{inj}(\mathcal{M})$ denotes the injectivity radius of \mathcal{M} . Because \mathcal{M} is closed, the injectivity radius is bounded away from 0.

Proposition 3.8. *In normal coordinates the metric has the following expansion:*

$$g_{kl}(x) = \delta_{kl} + \frac{1}{3}R_{ijkl}x^i x^j + O(|x|^3),$$

where $\delta_{kl} = 1$ if $k = l$ and is zero otherwise. Moreover, for any $v, w \in B(0, 1)$ and $r \leq \text{inj}(\mathcal{M})$:

$$d(\exp_p(rv), \exp_p(rw))^2 = r^2\|v - w\|^2 + \frac{r^4}{3}\langle R(w, v)w, v \rangle + O(r^5). \quad (16)$$

Proof. See the discussion in [41] above Theorem 5.5.8 and Exercises 5.9.26 and 5.9.27. \square

Combining (13) and (16) yields:

$$d(\exp_p(rv), \exp_p(rw))^2 = r^2 \|v - w\|^2 + \frac{r^4 K(v, w)}{3} (\|v\|^2 \|w\|^2 - \langle v, w \rangle^2) + O(r^5).$$

For any $x_i \in \mathcal{X}$ let $r_{x_i, k}$ denote the distance to the k NN of x_i . Because $r_{x_i, k} \rightarrow 0^+$ as $n \rightarrow \infty$, we have that $r_{x_i, k} \leq \text{inj}(\mathcal{M})$ for all x_i , almost surely for n large enough.

The proof of Theorem 3.9 proceeds in a similar manner to the proof of Theorem 3.7. However, care must be taken to account for the curvature. Note that for any quantity $c := c(n)$ implicitly dependent on n , we shall say that $c = o(1)$ if for any $\epsilon > 0$ there exists an N such that for all $n > N$ we have that $c(n) < \epsilon$.

Theorem 3.9. *Let (\mathcal{M}, g) be a closed and compact Riemannian manifold. Suppose that $\mathcal{X} = \{x_i\}_{i=1}^n$ are drawn i.i.d. from \mathcal{M} according to a probability distribution f . If*

$$k \geq 1 + (1 + o(1)) \frac{3f_{\max}}{f_{\min}} \left(\frac{(1 - o(1))^{2/p}}{4^{1/p}} - \frac{1}{4} \right)^{-d/2} \log(n),$$

then $\mathcal{G}_{\mathcal{M}, \mathcal{X}}^{p, k}$ is a 1-spanner of $\mathcal{G}_{\mathcal{M}, \mathcal{X}}^p$ with probability at least $1 - 1/n$ for n sufficiently large.

Proof. Assume that n is large enough such that $r_{x_i, k} \leq \text{inj}(\mathcal{M})$ for all x_i . Now consider a fixed x_i ; without loss of generality assume that it is x_1 . Let x_{i_1}, \dots, x_{i_k} denote the k NNs of x_1 , and consider any other $x_j \in \mathcal{X}$. Let \bar{x}_j denote the projection of x_j onto $B_d(x_1, r_{x_1, k})$. We shall show that, with high probability, there exists an $\ell \in \{1, 2, \dots, k\}$ such that: $d(x_1, x_{i_\ell})^p + d(x_{i_\ell}, \bar{x}_j)^p \leq d(x_1, \bar{x}_j)^p$. For convenience, let $r = d(x_1, \bar{x}_j) = r_{x_1, k}$ and let x_m denote the midpoint of the geodesic from x_1 to \bar{x}_j . Choose Riemannian normal coordinates centered at x_m such that $\bar{x}_j = \exp_{x_m}(\frac{r}{2}e_1)$ and $x_1 = \exp_{x_m}(-\frac{r}{2}e_1)$. For any $z \in B_d(x_m, r)$, we may write $z = \exp_{x_m}(rv)$ for some $v \in B(0, 1) \subset T_{x_m}\mathcal{M}$. Now, by (16)

$$\begin{aligned} d(x_1, z)^2 &= d\left(\exp_{x_m}\left(-\frac{r}{2}e_1\right), \exp_{x_m}(rv)\right)^2 \\ &= r^2 \left\| \frac{1}{2}e_1 + v \right\|^2 - \frac{r^4 K(e_1, v)}{3} \left(\frac{1}{4}\|v\|^2 - \frac{1}{4}\langle e_1, v \rangle^2 \right) + O(r^5) \\ &\leq r^2 \left\| \frac{1}{2}e_1 + v \right\|^2 - \frac{r^4 K_{\min}}{12} (\|v\|^2 - \langle e_1, v \rangle^2) + O(r^5) \end{aligned}$$

and similarly: $d(z, \bar{x}_j)^2 \leq r^2 \left\| -\frac{1}{2}e_1 + v \right\|^2 - \frac{r^4 K_{\min}}{12} (\|v\|^2 - \langle e_1, v \rangle^2) + O(r^5)$. We split the analysis into the case where $K_{\min} \geq 0$ and where $K_{\min} < 0$.

Case $K_{\min} \geq 0$ (Positive Sectional Curvature): If $K_{\min} \geq 0$ then the terms proportional to r^4 are strictly non-positive, and hence may be dropped. We get that:

$$d(x_1, z)^2 \leq r^2 \left\| \frac{1}{2}e_1 + v \right\|^2 + O(r^5) \text{ and } d(z, \bar{x}_j)^2 \leq r^2 \left\| -\frac{1}{2}e_1 + v \right\|^2 + O(r^5),$$

and hence $d(x_1, z)^p + d(z, \bar{x}_j)^p \leq r^p (\left\| \frac{1}{2}e_1 + v \right\|^p + \left\| -\frac{1}{2}e_1 + v \right\|^p) + O(r^{p+3})$. Thus, for r sufficiently small we may guarantee that

$$d(x_1, z)^p + d(z, \bar{x}_j)^p \leq d(x_1, \bar{x}_j)^p = r^p \leq d(x_1, x_j)^p \tag{17}$$

by ensuring that $\left\| \frac{1}{2}e_1 + v \right\|^p + \left\| -\frac{1}{2}e_1 + v \right\|^p \leq \alpha$, where $\alpha \in (0, 1)$ is such that the $O(r^{p+3})$ term is less than $(1 - \alpha)r^p$. As $r \rightarrow 0$ with $n \rightarrow \infty$, we observe that $\alpha = 1 - o(1)$.

Case $K_{\min} < 0$ (Negative Sectional Curvature): If $K_{\min} < 0$ then one can upper bound the terms proportional to r^4 by $-r^4 K_{\min}/12$ to obtain:

$$d(x_1, z)^2 \leq r^2 \left\| \frac{1}{2}e_1 + v \right\|^2 - \frac{r^4 K_{\min}}{12} + O(r^5) \text{ and } d(z, \bar{x}_j)^2 \leq r^2 \left\| -\frac{1}{2}e_1 + v \right\|^2 - \frac{r^4 K_{\min}}{12} + O(r^5).$$

and so:

$$\begin{aligned} d(x_1, z)^p + d(z, \bar{x}_j)^p &\leq r^p \left(\left\| \frac{1}{2}e_1 + v \right\|^p + \left\| -\frac{1}{2}e_1 + v \right\|^p \right) \\ &\quad + r^{p+2} \frac{-K_{\min}}{12} \left(\left\| \frac{1}{2}e_1 + v \right\|^{p-2} + \left\| -\frac{1}{2}e_1 + v \right\|^{p-2} \right) + O(r^{p+3}) \end{aligned} \quad (18)$$

As in the positive sectional curvature case, one can guarantee that:

$$d(x_1, z)^p + d(z, \bar{x}_j)^p \leq d(x_1, \bar{x}_j)^p = r^p \leq d(x_1, x_j)^p \quad (19)$$

by guaranteeing, for any $\alpha \in (0, 1)$, that:

$$\left\| \frac{1}{2}e_1 + v \right\|^p + \left\| -\frac{1}{2}e_1 + v \right\|^p \leq \alpha \quad (20)$$

as long as r is sufficiently small (equivalently, n is sufficiently large) that the $O(r^{p+2})$ term is less than $(1 - \alpha)r^p$. Again, we observe that $\alpha = 1 - o(1)$. Note that if (20) holds with $\alpha < 1$ then $\left\| \frac{1}{2}e_1 + v \right\|^{p-2} + \left\| -\frac{1}{2}e_1 + v \right\|^{p-2} < 1$, and so (18) becomes:

$$d(x_1, z)^p + d(z, \bar{x}_j)^p \leq \alpha r^p + \frac{-K_{\min}}{12} r^{p+2} + O(r^{p+3}). \quad (21)$$

For both cases, consider the p -elongated set defined in the tangent space:

$$\mathcal{D}_{\alpha,p} := \mathcal{D}_{\alpha,p} \left(\frac{1}{2}e_1, -\frac{1}{2}e_1 \right) = \left\{ v \in T_{x_m} \mathcal{M} \mid \left\| \frac{1}{2}e_1 + v \right\|^p + \left\| -\frac{1}{2}e_1 + v \right\|^p \leq \alpha \right\}$$

as well as its scaled image under the exponential map: $\exp(r\mathcal{D}_{\alpha,p})$. From the above arguments, (17) (resp. (19)) will hold as long as $z \in \exp(r\mathcal{D}_{\alpha,p})$. From Lemma 3.5, $\mathcal{D}_{\alpha,p}$ contains a ball of radius $\sqrt{\frac{\alpha^{2/p}}{4^{1/p}} - \frac{1}{4}}$, hence $r\mathcal{D}_{\alpha,p}$ contains a ball of radius $r_{\alpha,p}^* = r\sqrt{\frac{\alpha^{2/p}}{4^{1/p}} - \frac{1}{4}}$. It follows that the metric ball of radius $r_{\alpha,p}^*$ centered at x_m , namely $B_d(x_m, r_{\alpha,p}^*)$, is contained in $\exp(\mathcal{D}_{\alpha,p})$. As in the Euclidean case:

$$\begin{aligned} \mathbb{P} [x_{i_j} \in \exp(\mathcal{D}_{\alpha,p}) \mid x_{i_j} \in B_d(x_1, r)] &= \frac{\mathbb{P} [x_{i_j} \in \exp(\mathcal{D}_{\alpha,p})]}{\mathbb{P} [x_{i_j} \in B_d(x_1, r)]} \\ &\geq \frac{\mathbb{P} [x_{i_j} \in B_d(x_m, r_{\alpha,p}^*)]}{\mathbb{P} [x_{i_j} \in B_d(x_1, r)]} \geq \frac{f_{\min} V_{\min}(r_{\alpha,p}^*)}{f_{\max} V_{\max}(r)}. \end{aligned}$$

We now appeal to (14) and (15) as well as the fact that $r = o(1)$ to obtain:

$$\frac{V_{\min}(r_{\alpha,p}^*)}{V_{\max}(r)} = (1 - o(1)) \frac{(r_{\alpha,p}^*)^d}{r^d} = (1 - o(1)) \left(\frac{\alpha^{2/p}}{4^{1/p}} - \frac{1}{4} \right)^{d/2}$$

and so, recalling that $\alpha = 1 - o(1)$:

$$\mathbb{P} [x_{i_j} \in \exp(\mathcal{D}_{\alpha,p}) \mid x_{i_j} \in B_d(x_1, r)] \geq (1 - o(1)) \frac{f_{\min}}{f_{\max}} \left(\frac{(1 - o(1))^{2/p}}{4^{1/p}} - \frac{1}{4} \right)^{d/2}.$$

The same analysis as in the proof of Theorem 3.7 now applies, and for

$$k \geq 1 + (1 + o(1)) \frac{3f_{\max}}{f_{\min}} \left(\frac{(1 - o(1))^{2/p}}{4^{1/p}} - \frac{1}{4} \right)^{-d/2} \log(n),$$

we get that $\mathbb{P} [\mathcal{G}_{\mathcal{M},\mathcal{X}}^{p,k}$ is a 1-spanner of $\mathcal{G}_{\mathcal{M},\mathcal{X}}^p$] $\geq 1 - \frac{1}{n}$. \square

In the limit as the $o(1)$ terms become zero, we obtain $k \geq 1 + \frac{3f_{\max}}{f_{\min}} \left(\frac{4}{4^{1-1/p}-1} \right)^{d/2} \log(n)$ as in the isometrically embedded case.

3.3 Numerical Experiments

In this section we verify that the claimed dependence of k on n, p and d is indeed sufficient to ensure that $\mathcal{G}_{\mathcal{X}}^{p,k}$ is a 1-spanner of $\mathcal{G}_{\mathcal{X}}^p$. Our methodology is as follows:

- (1) For fixed p, d, \mathcal{M} and density $f(x)$, generate a sequence of (n, k) pairs.
- (2) For each pair (n, k) , we do the following:
 - (i) Generate a data set $\mathcal{X} = \{x_i\}_{i=1}^n$ by sampling i.i.d. according to $f(x)$ from \mathcal{M} .
 - (ii) For all pairs $\{x_i, x_j\}$ compute the PWSPD in the complete graph, $\ell_p(x_i, x_j)$, as well as in the k NN graph $\ell_p^{\mathcal{G}_{\mathcal{X}}^{p,k}}(x_i, x_j)$.
 - (iii) If $\max_{1 \leq i < j \leq n} \left| \ell_p(x_i, x_j) - \ell_p^{\mathcal{G}_{\mathcal{X}}^{p,k}}(x_i, x_j) \right| > 10^{-10}$ record “failure”; else, record “success”.
- (3) We repeat step 2 twenty times and compute the proportion of successes; see Figure 4.

As can be seen from the heatmaps in Figure 4, there is a sharp transition between an “all failures” and an “all successes” regime. This transition line is indeed roughly linear when viewed using semi-log-x axes, *i.e.* it obeys the relationship $k \propto \log(n)$. As pictured in Figure 4, we plot the empirically derived best approximation to this line. We observe that the slope of this line decreases with increasing p (compare heatmaps 1–3), as predicted by Theorem 3.7. One can also infer that this slope depends on the intrinsic dimension of the data, rather than ambient dimension, by observing that the slope is less in heatmap 4 than it is in heatmap 2, because the only difference between these settings is that for heatmap 4 the data is intrinsically four dimensional. Intriguingly, by comparing heatmaps 2 and 5 we see that drawing data from a Gaussian distribution instead of a uniform distribution seems to have little effect, suggesting that the implicit assumption $f_{\min} > 0$ in Theorems 3.7 and 3.9 is unnecessary. Finally, we note that in all cases the slope is smaller than predicted by Theorem 3.7. For example, for the first three cases, Theorem 3.7 predicts slopes of 363.02, 96 and 9.89 respectively while empirically we compute slopes of 43.43, 25.33 and 0.29.

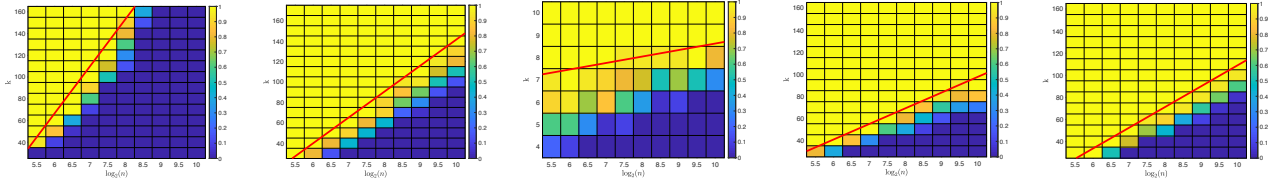


Figure 4: Heatmaps showing the proportion of randomly generated data sets for which $G_{\mathcal{X}}^{k,p}$ is a 1-spanner of $G_{\mathcal{X}}^p$. The first three heatmaps consider data uniformly drawn from $[0, 1]^5$, but with $p = 1.5, 2$ and 10 respectively. The fourth considers data drawn uniformly from the unit sphere $\mathbb{S}^4 \subset \mathbb{R}^5$ with $p = 2$. The fifth considers data drawn from the Gaussian distribution in \mathbb{R}^5 with mean $\mathbf{0}$ and covariance I with $p = 2$. The red line is the line of best fit through these lines, from left to right, are 43.43, 25.33, 0.29, 14.18 and 18.79

4 Global Analysis: Statistics on PWSPD and Percolation

We recall that after a suitable normalization, ℓ_p is a consistent estimator for \mathcal{L}_p (see Definition 1.2). Indeed, [32] proved that for any $d \geq 1$, $p > 1$, there exists a constant $C_{p,d}$ independent of n such that $\lim_{n \rightarrow \infty} \tilde{\ell}_p(x, y) = C_{p,d} \mathcal{L}_p(x, y)$. The important question then arises: how quickly does $\tilde{\ell}_p$ converge?

How large does n need to be to guarantee the error incurred by approximating \mathcal{L}_p with $\tilde{\ell}_p$ is small? To answer this question we turn to results from Euclidean first passage percolation (FPP) [29, 30, 5, 19]. For any discrete set X , we let $\ell_p(x, y, X)$ denote the PWSPD computed in the set $X \cup \{x, y\}$.

4.1 Overview of Euclidean First Passage Percolation

Euclidean FPP analyzes $\ell_p^p(0, z, H_1)$, where H_1 is a homogeneous, unit intensity Poisson point process (PPP) defined on all of \mathbb{R}^d .

Definition 4.1. A (homogeneous) Poisson point process (PPP) on \mathbb{R}^d is a point process such that for any bounded subset $A \subset \mathbb{R}^d$, the number of points in A , denoted n_A , is a random variable with distribution $\mathbb{P}(n_A = m) = \frac{1}{m!} (\lambda |A|)^m e^{-\lambda |A|}$. The parameter λ is the intensity of the PPP.

It is known that

$$\lim_{\|z\| \rightarrow \infty} \frac{\ell_p^p(0, z, H_1)}{\|z\|} = \mu, \quad (22)$$

where $\mu = \mu_{p,d}$ is a constant depending only on p, d known as the *time constant*. The convergence of $\ell_p^p(0, z, H_1)$ is studied by decomposing the error into random and deterministic fluctuations, i.e.

$$\ell_p^p(0, z, H_1) - \mu \|z\| = \underbrace{\ell_p^p(0, z, H_1) - \mathbb{E}[\ell_p^p(0, z, H_1)]}_{\text{random}} + \underbrace{\mathbb{E}[\ell_p^p(0, z, H_1)] - \mu \|z\|}_{\text{deterministic}}.$$

In terms of mean squared error (MSE), one has the standard bias-variance decomposition:

$$\mathbb{E} \left[(\ell_p^p(0, z, H_1) - \mu \|z\|)^2 \right] = (\mathbb{E}[\ell_p^p(0, z, H_1)] - \mu \|z\|)^2 + \text{Var}(\ell_p^p(0, z, H_1)).$$

The following Proposition is well known in the Euclidean FPP literature.

Proposition 4.2. Let $d \geq 2$ and $p > 1$. Then $\mathbb{E} \left[(\ell_p^p(0, z, H_1) - \mu \|z\|)^2 \right] \leq C \|z\| \log^2(\|z\|)$.

Proof. By Theorem 2.1 in [30], $\text{Var}(\ell_p^p(0, z, H_1)) \leq C\|z\|$. By Theorem 2.1 in [2],

$$(\mathbb{E}[\mu\|z\|] - \mu\|z\|)^2 \leq C\|z\| \log^2(\|z\|).$$

□

Although $\text{Var}(\ell_p^p(0, z, H_1)) \leq C\|z\|$ is the best bound which has been proved, the fluctuation rate is known to in fact depend on the dimension, i.e. $\text{Var}(\ell_p^p(0, z, H_1)) \sim \|z\|^{2\chi}$ for some exponent $\chi = \chi(d) \leq \frac{1}{2}$. Strong evidence is provided in [19] that the bias can be bounded by the variance, so the exponent χ very likely controls the total convergence rate.

The following tail bound is also known [30].

Proposition 4.3. *Let $d \geq 2, p > 1, \kappa_1 = \min\{1, d/p\}$, and $\kappa_2 = 1/(4p + 3)$. For any $\epsilon \in (0, \kappa_2)$, there exist constants C_0 and C_1 (depending on ϵ) such that for $\|z\| > 0$ and $\|z\|^{\frac{1}{2}+\epsilon} \leq \lambda \leq \|z\|^{\frac{1}{2}+\kappa_2-\epsilon}$, $\mathbb{P}(|\ell_p^p(0, z, H_1) - \mu\|z\|| \geq \lambda) \leq C_1 \exp\left(-C_0(\lambda/\sqrt{\|z\|})^{\kappa_1}\right)$.*

4.2 Convergence Rates for PWSPD

We wish to utilize the results in Section 4.1 to obtain convergence rates for PWSPD. However, we are interested in PWSPD computed on a compact set with boundary M and the convergence rate of ℓ_p rather than ℓ_p^p . To simplify the analysis, we restrict our attention to the following idealized model.

Assumption 1. *Let $M \subseteq \mathbb{R}^d$ be a convex, compact, d -dimensional set of unit volume containing the origin. Assume we sample n points independently and uniformly from M , i.e. $f = 1_M$, to obtain the discrete set \mathcal{X}_n . Let M_τ denote the points in M which are at least distance τ from the boundary of M , i.e. $M_\tau := \{x \in M : \min_{y \in \partial M} \|x - y\| > \tau\}$.*

We then establish three things: (i) Euclidean FPP results apply away from ∂M ; (ii) the time constant μ equals the constant $C_{p,d}$ in (3); (iii) ℓ_p has the same convergence rate as ℓ_p^p .

To establish (i), we let H_n denote a homogeneous PPP with rate $\lambda = n$, and let $\ell_p(0, y, H_n)$ denote the length of the shortest path connecting 0 and y in H_n . We also let $\mathcal{X}_N = H_n \cap M$ and $\ell_p(0, y, \mathcal{X}_N)$ denote the PWSPD in \mathcal{X}_N ; note $\mathbb{E}[|\mathcal{X}_N|] = n$. To apply percolation results to our setting, the statistical equivalence of $\ell_p(0, y, \mathcal{X}_n)$, $\ell_p(0, y, \mathcal{X}_N)$, and $\ell_p(0, y, H_n)$ must be established. For n large, the equivalence of $\ell_p(0, y, \mathcal{X}_n)$ and $\ell_p(0, y, \mathcal{X}_N)$ is standard and we omit any analysis. The equivalence of $\ell_p(0, y, \mathcal{X}_N)$ and $\ell_p(0, y, H_n)$ is less clear. In particular, how far away from ∂M do 0, y need to be to ensure these metrics are the same? The following proposition is a direct consequence of Theorem 2.4 from [30], and essentially guarantees the equivalence of the metrics as long as 0 and y are at least distance $O(n^{-\frac{1}{4d}})$ from ∂M .

Proposition 4.4. *Let $d \geq 2, p > 1, \kappa_1 = \min\{1, \frac{d}{p}\}$, $\kappa_2 = 1/(4p + 3)$, and $\epsilon \in (0, \frac{\kappa_2}{2})$, and $\tau = n^{-\frac{1}{4d} + \frac{\epsilon}{d}} \text{diam}(M)^{\frac{3}{4} + \epsilon}$. Then for all $0, y \in M_\tau$, the geodesics connecting 0, y in \mathcal{X}_N and H_n are equal with probability at least $1 - C_{1,\epsilon} \exp(-C_{0,\epsilon}(n^{\frac{1}{d}}\|y\|)^{\frac{3}{4}\epsilon\kappa_1})$, so that $\ell_p(0, y, \mathcal{X}_N) = \ell_p(0, y, H_n)$.*

Next we establish the equivalence of $\mu_{p,d}$ (percolation time constant) and $C_{p,d}$ (PWSPD discrete-to-continuum normalization constant).

Proposition 4.5. *Let $\mu_{p,d}$ be as in (22) and $C_{p,d}$ as in (3). Then $\mu_{p,d}^{1/p} = C_{p,d}$.*

Proof. Suppose Assumption 1 holds and choose $y \in M$ with $\|y\| = 1$ and let M be such that 0, y are not on the boundary. By Proposition 4.4, $\lim_{n \rightarrow \infty} \ell_p(0, y, \mathcal{X}_n) = \lim_{n \rightarrow \infty} \ell_p(0, y, H_n)$. Let H_1 be

the unit intensity PPP obtained from H_n by rescaling each axis by $n^{1/d}$, so that $\ell_p(0, y, H_n) = n^{-\frac{1}{d}} \ell_p(0, n^{\frac{1}{d}} y, H_1)$. For notational convenience, let $z = n^{\frac{1}{d}} y$. Then

$$\begin{aligned} \lim_{n \rightarrow \infty} \tilde{\ell}_p(0, y, \mathcal{X}_n) &= \lim_{n \rightarrow \infty} \tilde{\ell}_p(0, y, H_n) \\ &= \lim_{n \rightarrow \infty} n^{\frac{p-1}{pd}} \ell_p(0, y, H_n) \\ &= \lim_{n \rightarrow \infty} n^{\frac{p-1}{pd}} n^{-\frac{1}{d}} \ell_p(0, n^{\frac{1}{d}} y, H_1) \\ &= \lim_{\|z\| \rightarrow \infty} \|z\|^{\frac{p-1}{p}} \|z\|^{-1} \ell_p(0, z, H_1) \\ &= \lim_{\|z\| \rightarrow \infty} \frac{\ell_p(0, z, H_1)}{\|z\|^{1/p}}. \end{aligned}$$

Thus, $C_{p,d} = C_{p,d} \mathcal{L}_p(0, y) = \lim_{n \rightarrow \infty} \tilde{\ell}_p(0, y, \mathcal{X}_n) = \lim_{\|z\| \rightarrow \infty} \frac{\ell_p(0, z, H_1)}{\|z\|^{1/p}} = \mu_{p,d}^{1/p}$. \square

Finally, we bound our real quantity of interest: the convergence rate of $\tilde{\ell}_p$ to $C_{p,d} \mathcal{L}_p$.

Theorem 4.6. *Assume Assumption 1, $d \geq 2, p > 1, \kappa_2 = 1/(4p + 3), \tau = n^{-\frac{(1-\kappa_2)}{4d}} \text{diam}(M)^{\frac{3+\kappa_2}{4}}$, and $0, y \in M_\tau$. Then for n large enough, $\mathbb{E} \left[\left(\tilde{\ell}_p(0, y, \mathcal{X}_n) - C_{p,d} \mathcal{L}_p(0, y) \right)^2 \right] \lesssim n^{-\frac{1}{d}} \log^2(n)$.*

Proof. To simplify notation throughout the proof we denote $\mathcal{L}_p(0, y)$ simply by \mathcal{L}_p . By Proposition 4.5 and for n large enough,

$$\mathbb{E} \left[\left(\tilde{\ell}_p(0, y, \mathcal{X}_n) - C_{p,d} \mathcal{L}_p \right)^2 \right] \lesssim \mathbb{E} \left[\left(\tilde{\ell}_p(0, y, \mathcal{X}_N) - \mu^{1/p} \mathcal{L}_p \right)^2 \right] =: (I),$$

where $\mathcal{X}_N = H_n \cap M$ and H_n is a homogeneous PPP with rate n . Let A be the event that the geodesics from 0 to y in \mathcal{X}_N and H_n are equal. Since we assume $\tau = n^{-\frac{(1-\kappa_2)}{4d}} \text{diam}(M)^{\frac{3+\kappa_2}{4}}$, we may apply Proposition 4.4 with $\epsilon = \kappa_2/4$ to conclude $\mathbb{P}(A) \geq 1 - C_1 \exp\left(-C_0 \|y\|^{\frac{\alpha}{d}} n^\alpha\right)$ for $\alpha = \frac{3\kappa_2}{16} (1 \wedge \frac{d}{p})$.

Conditioning on A , and observing $\tilde{\ell}_p(0, y, \mathcal{X}_N) = n^{\frac{p-1}{pd}} \ell_p(0, y, \mathcal{X}_N) \leq n^{\frac{p-1}{pd}} \|y\|$, we obtain

$$\begin{aligned} (I) &= \mathbb{E} \left[\left(\tilde{\ell}_p(0, y, \mathcal{X}_N) - \mu^{1/p} \mathcal{L}_p \right)^2 \mid A \right] \mathbb{P}(A) + \mathbb{E} \left[\left(\tilde{\ell}_p(0, y, \mathcal{X}_N) - \mu^{1/p} \mathcal{L}_p \right)^2 \mid \bar{A} \right] \mathbb{P}(\bar{A}) \\ &\leq \mathbb{E} \left[\left(\tilde{\ell}_p(0, y, H_n) - \mu^{1/p} \mathcal{L}_p \right)^2 \mid A \right] + \left(n^{\frac{2(p-1)}{pd}} \|y\|^2 + \mu^{2/p} \mathcal{L}_p^2 \right) C_1 \exp\left(-C_0 \|y\|^{\frac{\alpha}{d}} n^\alpha\right) \\ &\leq \mathbb{E} \left[\left(\tilde{\ell}_p(0, y, H_n) - \mu^{1/p} \mathcal{L}_p \right)^2 \right] + q_1 \end{aligned}$$

where q_1 decays exponentially in n (for the last line note that conditioning on A means conditioning on the geodesics being local, which can only decrease the expected error).

A Lipschitz analysis applied to the function $g(x) = x^{1/p}$ yields:

$$\left(\tilde{\ell}_p(0, y, H_n) - \mu^{1/p} \mathcal{L}_p \right)^2 \leq p^{-2} \tilde{\ell}_p(0, y, H_n)^{2(1-p)/p} \cdot \left(\tilde{\ell}_p^p(0, y, H_n) - \mu \mathcal{L}_p^p \right)^2.$$

By Proposition 4.3,

$$\tilde{\ell}_p^p(0, y, H_n) \geq \mu \mathcal{L}_p^p - \frac{\|y\|^{\frac{1}{2}+\epsilon}}{n^{\frac{1}{d}(\frac{1}{2}-\epsilon)}} \quad (23)$$

with probability at least $1 - C_1 \exp\left(-C_0 \|y\|^{\epsilon \kappa_1} n^{\frac{\epsilon \kappa_1}{d}}\right)$ for any $\epsilon \in (0, \kappa_2)$, where $\kappa_1 = \min\{1, d/p\}$. Fix $\epsilon \in (0, \kappa_2)$ and let B be the event that (23) is satisfied. On B ,

$$\begin{aligned} \tilde{\ell}_p(0, y, H_n)^{\frac{2(1-p)}{p}} &\leq (\mu^{1/p} \mathcal{L}_p)^{\frac{2(1-p)}{p}} \left(1 - \frac{\|y\|^{\frac{1}{2}+\epsilon}}{\mu \mathcal{L}_p^p n^{\frac{1}{d}(\frac{1}{2}-\epsilon)}}\right)^{\frac{2(1-p)}{p^2}} \\ &\leq (\mu^{1/p} \mathcal{L}_p)^{\frac{2(1-p)}{p}} \left(1 + \frac{2(p-1)\|y\|^{\frac{1}{2}+\epsilon}}{p^2 \mu \mathcal{L}_p^p n^{\frac{1}{d}(\frac{1}{2}-\epsilon)}} + \text{higher order terms}\right) \\ &\leq 2(\mu^{1/p} \mathcal{L}_p)^{\frac{2(1-p)}{p}}, \end{aligned}$$

for n large enough. Note also that

$$\mathbb{E} \left[\left(\tilde{\ell}_p(0, y, H_n) - \mu^{1/p} \mathcal{L}_p \right)^2 \mid \bar{B} \right] \mathbb{P}(\bar{B}) \leq \left(n^{\frac{2(p-1)}{pd}} \|y\|^2 + \mu^{2/p} \mathcal{L}_p^2 \right) \exp\left(-C_0 \|y\|^{\epsilon \kappa_1} n^{\frac{\epsilon \kappa_1}{d}}\right) := q_2$$

and q_2 decreases exponentially in n . We thus obtain

$$\begin{aligned} \mathbb{E} \left[\left(\tilde{\ell}_p(0, y, H_n) - \mu^{1/p} \mathcal{L}_p \right)^2 \right] &\leq \mathbb{E} \left[\left(\tilde{\ell}_p(0, y, H_n) - \mu^{1/p} \mathcal{L}_p \right)^2 \mid B \right] \mathbb{P}(B) + q_2 \\ &\leq \frac{2}{p^2} (\mu^{1/p} \mathcal{L}_p)^{\frac{2(1-p)}{p}} \mathbb{E} \left[\left(\tilde{\ell}_p^p(0, y, H_n) - \mu \mathcal{L}_p^p \right)^2 \mid B \right] + q_2 \\ &= K \mathbb{E} \left[\left(\tilde{\ell}_p^p(0, y, H_n) - \mu \mathcal{L}_p^p \right)^2 \right] + q_2 \end{aligned}$$

where K is a constant depending on $p, d, \|y\|$, and the last line follows since once again the expected error is lower conditioned on B than unconditionally. We have thus established

$$\mathbb{E} \left[\left(\tilde{\ell}_p(0, y, \mathcal{X}_n) - C_{p,d} \mathcal{L}_p \right)^2 \right] \lesssim \mathbb{E} \left[\left(\tilde{\ell}_p^p(0, y, H_n) - \mu \mathcal{L}_p^p \right)^2 \right] + q_1 + q_2$$

for q_1, q_2 exponentially small in n . Finally let H_1 be the unit intensity homogeneous PPP obtained from H_n by multiplying each axis by $n^{1/d}$. By Proposition 4.2,

$$\begin{aligned} &\mathbb{E} \left[\left(\ell_p^p(0, n^{\frac{1}{d}} y, H_1) - \mu n^{\frac{1}{d}} \|y\| \right)^2 \right] \lesssim n^{\frac{1}{d}} \|y\| \log^2(n^{\frac{1}{d}} \|y\|) \\ \Rightarrow &\mathbb{E} \left[\left(n^{\frac{p}{d}} \ell_p^p(0, y, H_n) - n^{\frac{1}{d}} \mu \mathcal{L}_p^p \right)^2 \right] \lesssim n^{\frac{1}{d}} \|y\| \log^2(n^{\frac{1}{d}} \|y\|) \\ \Rightarrow &\mathbb{E} \left[\left(n^{\frac{p-1}{d}} \ell_p^p(0, y, H_n) - \mu \mathcal{L}_p^p \right)^2 \right] \lesssim n^{-\frac{1}{d}} \|y\| \log^2(n^{\frac{1}{d}} \|y\|) \\ \Rightarrow &\mathbb{E} \left[\left(\tilde{\ell}_p^p(0, y, H_n) - \mu \mathcal{L}_p^p \right)^2 \right] \lesssim n^{-\frac{1}{d}} \log^2(n). \end{aligned}$$

For n large enough, the above dominates q_1, q_2 , so that

$$\mathbb{E} \left[\left(\tilde{\ell}_p(0, y, \mathcal{X}_n) - C_{p,d} \mathcal{L}_p \right)^2 \right] \leq K n^{-\frac{1}{d}} \log^2(n)$$

for a constant K depending on $p, d, \|y\|$. □

4.3 Estimating the Fluctuation Exponent

As an application, we utilize the 1-spanner results of Section 3 to empirically estimate the fluctuation rate $\chi(d)$. Since there is evidence that the variance dominates the bias, this important parameter very likely determines the convergence rate of $\tilde{\ell}_p$ to \mathcal{L}_p . Once again utilizing the change of variable $z = n^{\frac{1}{d}}y$, we note

$$\text{Var} [\ell_p^p(0, z, H_1)] \lesssim \|z\|^{2\chi} \iff \text{Var} [\tilde{\ell}_p(0, y, \mathcal{X}_n)] \lesssim n^{\frac{2(\chi-1)}{d}},$$

and we estimate the right hand side from simulations. Specifically, we sample n points uniformly from the unit cube $[0, 1]^d$ and compute $\tilde{\ell}_p(x, y, \mathcal{X}_n)$ for $x = (0.25, 0.5, \dots, 0.5)$, $y = (0.75, 0.5, \dots, 0.5)$ in a k NN graph on \mathcal{X}_n , with $k = \lceil 1 + 3 \left(\frac{4}{4^{1-1/p}-1} \right)^{d/2} \log(n) \rceil$ as required by Theorem 3.7. We vary n from $n_{\min} = 11,586$ to $n_{\max} = 92,682$, and for each n we estimate $\text{Var} [\tilde{\ell}_p(x, y, \mathcal{X}_n)]$ from S simulations. Figure 5 shows the resulting log-log variance plots for $d = 2, 3, 4$ and various p , as well as the slopes m from a linear regression. The observed slopes are related to χ by $\chi = md/2 + 1$, and one thus obtains the estimates for χ reported in Table 2.

These simulations confirm that χ is indeed independent of p . It is conjectured in the percolation literature that $\chi(d) \rightarrow 0^+$ as d increases, with $\chi(2) = \frac{1}{3}$, $\chi(3) \approx \frac{1}{4}$, which is consistent with our results. For $d = 2$, the empirical convergence rate is thus $n^{-\frac{2}{3}}$ (not $n^{-\frac{1}{2}}$ as given in Theorem 4.6), and for large d one expects an MSE of order $n^{-\frac{2}{d}}$ instead of $n^{-\frac{1}{d}}$. However estimating χ empirically becomes increasingly difficult as d increases, since one has less sparsity in the k NN graph, and because χ is obtained from m by $\chi = md/2 + 1$, so errors incurred in estimating the regression slopes are amplified by a factor of d . Table 2 also reports the factors n_{\min}/k and n_{\max}/k , which can be interpreted as the expected computational speed-up obtained by running the simulation in a k NN graph instead of a complete graph. We were unable to obtain empirical speed-up factors since computational resources prevented running the simulations in a complete graph, even for n_{\min} .

An important open problem is establishing that $\tilde{\ell}_p$ computed from a nonuniform density enjoys the same convergence rate (with respect to n) as the uniform case. Although this seems intuitively true and preliminary simulation results support this equivalence, to the best of our knowledge it has not been proven, as the current proof techniques rely on “straight line” geodesics.

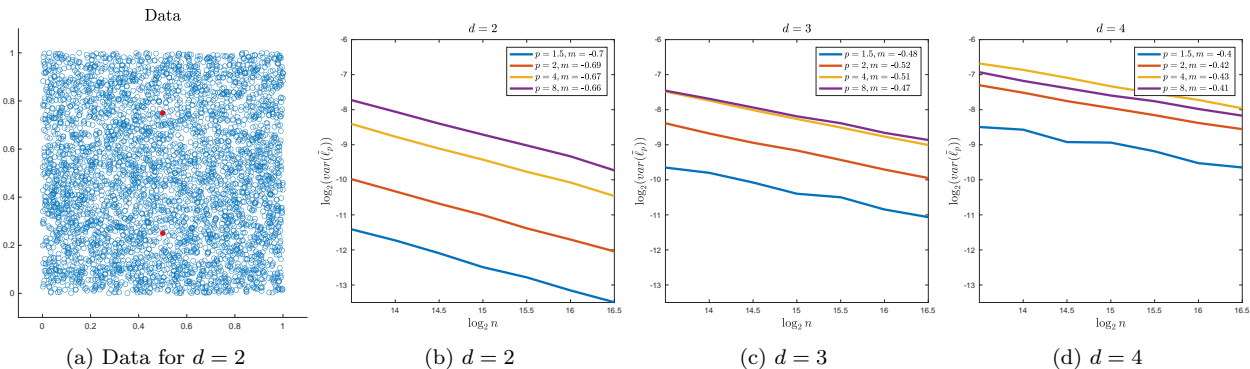


Figure 5: Variance plots for $\tilde{\ell}_p$. For each n , the variance was estimated from a maximum of $S = 24000$ simulations, with a smaller S when p was small and/or the dimension was large. Specifically, when $d = 2$, $S = 14000$ was used for $p = 1.5$; when $d = 3$, $S = 5000, 12000$ was used for $p = 1.5, 2$; when $d = 4$, $S = 2000, 6000, 19000$ was used for $p = 1.5, 2, 4$.

		$\hat{\chi}$	CI for χ	n_{\min}/k	n_{\max}/k
$d = 2$	$p = 1.5$	0.30	(0.28, 0.32)	60	394
	$p = 2$	0.31	(0.30, 0.32)	102	667
	$p = 4$	0.33	(0.31, 0.34)	184	1204
	$p = 8$	0.34	(0.32, 0.37)	236	1545
$d = 3$	$p = 1.5$	0.28	(0.20, 0.36)	23	152
	$p = 2$	0.23	(0.20, 0.25)	51	336
	$p = 4$	0.24	(0.22, 0.25)	126	820
	$p = 8$	0.29	(0.27, 0.32)	184	1204
$d = 4$	$p = 1.5$	0.19	(0.03, 0.36)	9	58
	$p = 2$	0.16	(0.13, 0.19)	26	169
	$p = 4$	0.14	(0.11, 0.18)	85	558
	$p = 8$	0.19	(0.14, 0.23)	141	927

Table 2: The slopes of $\log(n)$ versus $\text{Var}(\tilde{\ell}_p)$ are shown for uniform data for different density weightings (p) and different dimensions (d).

5 Conclusion and Future Work

This article establishes the local equivalence of PWSPD to a density-based stretch of Euclidean distance; kernels constructed with PWSPD strengthen connections in high-density regions, in contrast to many popular machine learning kernels which strengthen connections in low-density regions (e.g. self-tuning spectral clustering, diffusion maps). We derive a near-optimal condition on k for the k NN graph to be a 1-spanner for the PWSPD. This condition quantifies the dependence on p and improves the dimensional dependence, and allows for PWSPDs to be computed efficiently in a sparse graph. Moreover, we leverage the theory of Euclidean first passage percolation to establish statistical convergence rates for the PWSPD to its continuum limit, and apply our spanner results to empirically support conjectures regarding the optimal dimension-dependent rates of convergence.

Many directions remain for future work. Our statistical convergence rates for PWSPD in Section 4 are limited to uniform distributions. Preliminary numerical experiments indicate that these rates also hold for PWSPDs computed from a varying density. However proving such a result is non-trivial since it requires analysis of nonhomogenous PPPs, and rigorous convergence rates for nonhomogeneous PPPs are lacking in the literature.

The analysis of Section 2 proved the local equivalence of PWSPDs with density-stretched Euclidean distances. In addition to being of interest in their own right, these results and the convergence results of Section 4 are the first steps in a program of developing a discrete-to-continuum limit analysis for PWSPDs. That is, one can build operators (e.g. graph Laplacians) using $\tilde{\ell}_p$ and then allow $n \rightarrow \infty$. A major problem is to develop conditions (e.g. on the kernel scaling parameter) so that the graph Laplacian (defined with $\tilde{\ell}_p$) converges to a continuum Laplacian (defined with \mathcal{L}_p).

The numerical results of Section 3.3 confirm that $k \propto \log(n)$ is required for the k NN graph to be a 1-spanner, as predicted by theory. However, these same experiments also suggest that the *constants of proportionality* given by Theorems 3.7 and 3.9 are pessimistic. It is of interest to develop alternative approaches that yield sharper bounds.

Another future direction is the analysis of how data clusterability with PWSPDs depends on p for various random data models. PWSPD is a useful metric for spectral clustering, but the optimal weight parameter p depends on the data application (see Figures 1-3). Precise models of data clusterability based on density in the context of spectral clustering have been developed in the

discrete [34] and continuum [28] settings, but not for clustering with general PWSPD. Future work will explore both theoretical guarantees for clusterability with PWSPD and the optimal choice of p in specific applications such as single cell RNA sequence data.

Relatedly, the results of this article are focused on the case when data is generated from a distribution supported exactly on a low-dimensional manifold \mathcal{M} . An arguably more realistic setting is the noisy one in which the data is distributed only approximately on \mathcal{M} . Topics of interest include how sensitive PWSPDs are to noise, robust denoising procedures which improve the accuracy of PWSPD computations, computing PWSPDs after dimension reduction, and which type of noise distributions are most adversarial to PWSPD. Indeed, bounded uniform noise may behave differently from Gaussian noise especially for large p , because PWSPD focuses on high-density regions for large p .

Acknowledgements

AVL acknowledges partial support from the US National Science Foundation under grant DMS-1912906. DM acknowledges partial support from the US National Science Foundation under grant DMS-1720237 and the Office of Naval Research under grant N000141712162. JMM acknowledges partial support from the US National Science Foundation under grants DMS-1912737 and DMS-1924513. DM thanks Matthias Wink for several useful discussions on Riemannian geometry.

References

- [1] M. Alamgir and U. Von Luxburg. Shortest path distance in random k-nearest neighbor graphs. In *ICML*, pages 1251–1258, 2012.
- [2] K.S. Alexander. A note on some rates of convergence in first-passage percolation. *The Annals of Applied Probability*, pages 81–90, 1993.
- [3] H. Antil, T. Berry, and J. Harlim. Fractional diffusion maps. *arXiv preprint arXiv:1810.03952*, 2018.
- [4] E. Arias-Castro. Clustering based on pairwise distances when the data is of mixed dimensions. *IEEE Transactions on Information Theory*, 57(3):1692–1706, 2011.
- [5] A. Auffinger, M. Damron, and J. Hanson. *50 Years of First-Passage Percolation*, volume 68. American Mathematical Soc., 2017.
- [6] M. Azizyan, A. Singh, and L. Wasserman. Density-sensitive semisupervised inference. *The Annals of Statistics*, 41(2):751–771, 2013.
- [7] M. Belkin and P. Niyogi. Laplacian eigenmaps for dimensionality reduction and data representation. *Neural Computation*, 15(6):1373–1396, 2003.
- [8] M. Belkin and P. Niyogi. Convergence of Laplacian eigenmaps. In *NIPS*, pages 129–136, 2007.
- [9] R.E. Bellman. *Adaptive control processes: a guided tour*. Princeton University Press, 2015.
- [10] T. Berry and T. Sauer. Local kernels and the geometric structure of data. *Applied and Computational Harmonic Analysis*, 40(3):439–469, 2016.

- [11] A.S. Bijral, N. Ratliff, and N. Srebro. Semi-supervised learning with density based distances. In *UAI*, pages 43–50, 2011.
- [12] E. Borghini, X. Fernández, P. Groisman, and G. Mindlin. Intrinsic persistent homology via density-based metric learning. *arXiv preprint arXiv:2012.07621*, 2020.
- [13] O. Bousquet, O. Chapelle, and M. Hein. Measure based regularization. In *NIPS*, pages 1221–1228, 2004.
- [14] H. Chang and D.-Y. Yeung. Robust path-based spectral clustering. *Pattern Recognition*, 41(1):191–203, 2008.
- [15] Y. Cheng. Mean shift, mode seeking, and clustering. *IEEE Transactions on Pattern Analysis and Machine Intelligence*, 17(8):790–799, 1995.
- [16] T. Chu, G.L. Miller, and D.R. Sheehy. Exact computation of a manifold metric, via Lipschitz embeddings and shortest paths on a graph. In *SODA*, pages 411–425, 2020.
- [17] R.R. Coifman and S. Lafon. Diffusion maps. *Applied and Computational Harmonic Analysis*, 21(1):5–30, 2006.
- [18] R.R. Coifman, S. Lafon, A.B. Lee, M. Maggioni, B. Nadler, F. Warner, and S.W. Zucker. Geometric diffusions as a tool for harmonic analysis and structure definition of data: Diffusion maps. *Proceedings of the National Academy of Sciences*, 102(21):7426–7431, 2005.
- [19] M. Damron and X. Wang. Entropy reduction in Euclidean first-passage percolation. *Electronic Journal of Probability*, 21, 2016.
- [20] L.P. Devroye and T.J. Wagner. The strong uniform consistency of nearest neighbor density estimates. *The Annals of Statistics*, pages 536–540, 1977.
- [21] D.L. Donoho and C. Grimes. Hessian eigenmaps: Locally linear embedding techniques for high-dimensional data. *Proceedings of the National Academy of Sciences*, 100(10):5591–5596, 2003.
- [22] M. Ester, H.-P. Kriegel, J. Sander, and X. Xu. A density-based algorithm for discovering clusters in large spatial databases with noise. In *KDD*, volume 96, pages 226–231, 1996.
- [23] A.M. Farahmand, C. Szepesvári, and J.-Y. Audibert. Manifold-adaptive dimension estimation. In *ICML*, pages 265–272, 2007.
- [24] B. Fischer, T. Zöllner, and J.M. Buhmann. Path based pairwise data clustering with application to texture segmentation. In *International Workshop on Energy Minimization Methods in Computer Vision and Pattern Recognition*, pages 235–250. Springer, 2001.
- [25] A. Gray. The volume of a small geodesic ball of a Riemannian manifold. *The Michigan Mathematical Journal*, 20(4):329–344, 1974.
- [26] P. Groisman, M. Jonckheere, and F. Sapienza. Nonhomogeneous Euclidean first-passage percolation and distance learning. *arXiv preprint arXiv:1810.09398*, 2018.
- [27] L. Györfi, M. Kohler, A. Krzyzak, and H. Walk. *A distribution-free theory of nonparametric regression*. Springer Science & Business Media, 2006.

- [28] F. Hoffmann, B. Hosseini, A.A. Oberai, and A.M. Stuart. Spectral analysis of weighted Laplacians arising in data clustering. *arXiv preprint arXiv:1909.06389*, 2019.
- [29] C.D. Howard and C.M. Newman. Euclidean models of first-passage percolation. *Probability Theory and Related Fields*, 108(2):153–170, 1997.
- [30] C.D. Howard and C.M. Newman. Geodesics and spanning trees for Euclidean first-passage percolation. *Annals of Probability*, pages 577–623, 2001.
- [31] G. Hughes. On the mean accuracy of statistical pattern recognizers. *IEEE Transactions on Information Theory*, 14(1):55–63, 1968.
- [32] S.J. Hwang, S.B. Damelin, and A. Hero. Shortest path through random points. *The Annals of Applied Probability*, 26(5):2791–2823, 2016.
- [33] D.B. Johnson. Efficient algorithms for shortest paths in sparse networks. *Journal of the ACM*, 24(1):1–13, 1977.
- [34] A. Little, M. Maggioni, and J.M. Murphy. Path-based spectral clustering: Guarantees, robustness to outliers, and fast algorithms. *Journal of Machine Learning Research*, 21(6):1–66, 2020.
- [35] D.O. Loftsgaarden and C.P. Quesenberry. A nonparametric estimate of a multivariate density function. *The Annals of Mathematical Statistics*, 36(3):1049–1051, 1965.
- [36] P. C. Mahalanobis. On the generalized distance in statistics. *National Institute of Science of India*, 1936.
- [37] J. Malik, C. Shen, H.-T. Wu, and N. Wu. Connecting dots: from local covariance to empirical intrinsic geometry and locally linear embedding. *Pure and Applied Analysis*, 1(4):515–542, 2019.
- [38] D. Mckenzie and S. Damelin. Power weighted shortest paths for clustering Euclidean data. *Foundations of Data Science*, 1(3):307, 2019.
- [39] A. Moscovich, A. Jaffe, and B. Nadler. Minimax-optimal semi-supervised regression on unknown manifolds. In *AISTATS*, pages 933–942, 2017.
- [40] A.Y. Ng, M.I. Jordan, and Y. Weiss. On spectral clustering: Analysis and an algorithm. In *NIPS*, pages 849–856, 2002.
- [41] P. Petersen, S. Axler, and K.A. Ribet. *Riemannian Geometry*, volume 171. Springer, 2006.
- [42] A. Rinaldo and L. Wasserman. Generalized density clustering. *The Annals of Statistics*, 38(5):2678–2722, 2010.
- [43] A. Rodriguez and A. Laio. Clustering by fast search and find of density peaks. *Science*, 344(6191):1492–1496, 2014.
- [44] Sajama and A. Orlitsky. Estimating and computing density based distance metrics. In *ICML*, pages 760–767, 2005.
- [45] L.K. Saul and M.I. Jordan. A variational principle for model-based interpolation. In *NIPS*, pages 267–273, 1997.
- [46] G. Schiebinger, M.J. Wainwright, and B. Yu. The geometry of kernelized spectral clustering. *The Annals of Statistics*, 43(2):819–846, 2015.

- [47] J. Shi and J. Malik. Normalized cuts and image segmentation. *IEEE Transactions on Pattern Analysis and Machine Intelligence*, 22(8):888–905, 2000.
- [48] J.B. Tenenbaum, V. De Silva, and J.C. Langford. A global geometric framework for nonlinear dimensionality reduction. *Science*, 290(5500):2319–2323, 2000.
- [49] L. van der Maaten and G. Hinton. Visualizing data using t-SNE. *Journal of Machine Learning Research*, 9(Nov):2579–2605, 2008.
- [50] P. Vincent and Y. Bengio. Density-sensitive metrics and kernels. In *Snowbird Learning Workshop*, 2003.
- [51] U. Von Luxburg. A tutorial on spectral clustering. *Statistics and Computing*, 17(4):395–416, 2007.
- [52] L. Zelnik-Manor and P. Perona. Self-tuning spectral clustering. In *NIPS*, pages 1601–1608, 2005.
- [53] S. Zhang and J.M. Murphy. Hyperspectral image clustering with spatially-regularized ultrametrics. *arXiv preprint arXiv:2004.05048*, 2020.